Available online at www.sciencedirect.com
ScienceDirect
Physica D 237 (2008) 2167–2183
PHYSICA D
www.elsevier.com/locate/physd

The state of the art in hydrodynamic turbulence: Past successes and future challenges

Itamar Procaccia[a,*], K.R. Sreenivasan[b]

[a] *Department of Chemical Physics, The Weizmann Institute of Science, Rehovot 76100, Israel*
[b] *International Centre for Theoretical Physics, Strada Costiera 11, 34014 Trieste, Italy*

Available online 6 February 2008

Abstract

We present a personal view of the state of the art in turbulence research. We summarize first the main achievements of the recent past, and then point ahead to the main challenges that remain for experimental and theoretical efforts.

Keywords: Anomalous scaling; Anisotropic and wall turbulence; Drag reduction; Convective and superfluid turbulence

1. Introduction

"The problem of turbulence" is often hailed as one of the last open problems of classical physics. In fact, there is no single "problem of turbulence"; rather, there are many inter-related problems, some of which have seen significant progress in recent years, and some are still open and inviting further research. The aim of this short review is to explain where fundamental progress has been made and where, in the opinion of the present writers, there are opportunities for further research.

There are many ways to set a fluid into turbulent motion. Examples include creating a large pressure gradient in a channel or a pipe, pulling a grid through a fluid, moving one or more boundaries to create a high shear and forcing a high thermal gradient. Customarily the vigor of forcing is measured by the Reynolds number Re, defined as $Re \equiv UL/\nu$ where L is the scale of the forcing, U is the characteristic velocity of the fluid at that same scale, and ν is the kinematic viscosity. The higher the Reynolds number the larger is the range of scales involved in the turbulent motion, roughly from the scale L itself (known as the "outer" or "integral" scale) down to the so-called "viscous" scale η which decreases as $Re^{-3/4}$ [1]. For large Re a turbulent flow exhibits an erratic dependence of the velocity field on the position in the fluid and on time. For this reason it is universally accepted that a statistical description of turbulence is called for, such that the objects of interest are almost invariably mean quantities (over time, space or an ensemble, depending on the application), fluctuations about the mean quantities, and correlation functions defined by these fluctuations; precise definitions will be given below. The crucial scientific questions thus deal typically with the universality of the statistical objects, universality with respect to the change of the fluid, or universality with respect to the change of forcing mechanisms. We will see that this universality issue binds together the various aspects of turbulence to be discussed below into a common quest – the quest for understanding those aspects of the phenomenon that transcend particular examples. We will strive to underline instances when this quest has been successful and when doubts remain.

The structure of this review is as follows: in Section 2 we discuss the statistical theory of homogeneous and isotropic turbulence and focus on the anomalous scaling exponents of correlation functions. For a part of the community this represented *the* important open problem in turbulence, and indeed great progress has been achieved here. In Section 3 we address homogeneous but anisotropic turbulence and present recent progress in understanding how to extract information about isotropic statistical objects, and how to characterize the anisotropic contributions. Section 4 deals with wall-bounded turbulence where both isotropy and homogeneity are lost (this

* Corresponding author.
E-mail address: itamar.procaccia@weizmann.ac.il (I. Procaccia).

0167-2789/$ - see front matter © 2008 Elsevier B.V. All rights reserved.
doi:10.1016/j.physd.2008.01.025

being the norm in practice, rather than the exception). We focus on the controversial issue of the log versus power-laws, clarifying the scaling assumptions underlying each of these approaches and replacing them by a universal scaling function; we show that this achieves an excellent modeling of channel or pipe flows. In Section 5 we consider turbulence with additives (like polymers or bubbles) and review the progress in understanding drag reduction by such additives. Section 6 discusses problems in thermal convection, with emphasis on recent work. Finally, Section 7 provides a selective account of the problems that have come to the fore in superfluid turbulence, sometimes bearing directly on its classical counterpart. The article concludes with a summary of the outlook.

2. Anomalous scaling in homogeneous and isotropic turbulence

A riddle of central interest for more than half a century to the theorist and the experimentalist alike concerns the numerical values of the scaling exponents that characterize the correlation and structure functions in homogeneous and isotropic turbulence. Before stating the problem one should note again that strictly homogeneous and isotropic state of a turbulent flow is not achievable in experiments; typically the same forcing mechanism that creates the turbulent flow is also responsible for breaking homogeneity or isotropy. Nevertheless, some reasonable approximations have been created in the laboratory. To get an even closer approximation, one has to resort to numerical simulations. For a long time, the Reynolds number of simulations was limited by numerical resolution and by storage capabilities, but this situation has improved tremendously in the past few years. Indeed, as an idealized state of turbulence which incorporates the essentials of the nonlinear transfer of energy among scales, homogeneous and isotropic turbulence has gained a time-honored status in the history of turbulence research, since its introduction by Taylor [2].

Consider then the velocity field $\boldsymbol{u}(\boldsymbol{r}, t)$ which satisfies the Navier–Stokes equations

$$\frac{\partial \boldsymbol{u}}{\partial t} + \boldsymbol{u} \cdot \nabla \boldsymbol{u} = -\nabla p + \nu \nabla^2 \boldsymbol{u} + \boldsymbol{f}, \tag{1}$$

where p is the pressure and $\boldsymbol{f}$ the (isotropic and homogeneous) forcing that creates the (isotropic and homogeneous) turbulent flow. Defining by $\langle \ldots \rangle$ an average over time, we realize that $\langle \boldsymbol{u} \rangle = 0$ everywhere in this flow. On the other hand, correlations of $\boldsymbol{u}$ are of interest, and we define the so-called "unfused" nth-order correlation function $\boldsymbol{T}_n$ as

$$\boldsymbol{T}_n(\boldsymbol{r}_1, t_1, \boldsymbol{r}_2, t_2, \ldots \boldsymbol{r}_n, t_n) \equiv \langle \boldsymbol{u}(\boldsymbol{r}_1, t_1) \boldsymbol{u}(\boldsymbol{r}_2, t_2) \ldots \boldsymbol{u}(\boldsymbol{r}_n, t_n) \rangle. \tag{2}$$

When all the times t_i are the same, $t_i = t$, we get the equal-time correlation function $\boldsymbol{F}_n(\boldsymbol{r}_1, \boldsymbol{r}_2, \ldots \boldsymbol{r}_n)$ which, for a forcing that is stationary in time, is a time-independent function of the $n(n-1)/2$ distances between the points of measurements, due to homogeneity. An even more contracted object is the so-called "longitudinal structure function" S_n,

$$S_n(R) \equiv \langle \{ [\boldsymbol{u}(\boldsymbol{r} + \boldsymbol{R}, t) - \boldsymbol{u}(\boldsymbol{r}, t)] \cdot \boldsymbol{R}/R \}^n \rangle, \tag{3}$$

which can be obtained by sums and differences of correlation functions $\boldsymbol{F}_n$, together with some fusion of coordinates [3]. On the basis of evidence from experiments and simulations, it has been stipulated (although never proven) that S_n is a homogeneous function of its arguments when the distance R is within the so-called "inertial range" $\eta \ll R \ll L$ in the sense that

$$S_n(\lambda R) = \lambda^{\zeta_n} S_n(R). \tag{4}$$

A central question concerns the numerical values of the "scaling exponents" ζ_n and their universality with respect to the nature of the forcing f. Even if we set aside questions about the form of $S_n(R)$, the question on exponents poses serious difficulties since it is impossible to derive a closed-form theory for the general structure function S_n, since any such theory involves higher-order unfused correlation functions with integrations over the time variable [4,5].

A closely related question with lesser theoretical difficulties pertains to other fields that couple to the velocity field, with the "passive scalar" case drawing most attention during the nineties. A passive scalar $\phi(\boldsymbol{r}, t)$ is a field that is advected by a turbulent velocity which itself is unaffected by it. For example,

$$\frac{\partial \phi}{\partial t} + \boldsymbol{u} \cdot \nabla \phi = \kappa \nabla^2 \phi + f. \tag{5}$$

If $\boldsymbol{u}$ and f are homogeneous and isotropic, and $Re \to \infty$ and $\kappa \to 0$, the structure functions $\mathcal{S}_n \equiv \langle [\phi(\boldsymbol{r} + \boldsymbol{R}) - \phi(\boldsymbol{r})]^n \rangle$ are stipulated to be homogeneous functions of their arguments with scaling exponents ξ_n.

Dimensional considerations predict $\zeta_n = \xi_n = n/3$, with $\zeta_3 = 1$ being an exact result from fluid mechanics, going back to Kolmogorov [6]. Experimental and simulations data deviated from these predictions (except, of course, for $n = 3$), and a hot pursuit for an example where these exponents could be calculated theoretically was inevitable. The first example that yielded to analysis was the Kraichnan model [7], in which $\boldsymbol{u}$ is not a generic velocity field, but rather a random Gaussian field whose second-order structure function scales with a scaling exponent ζ_2 as in Eq. (4), but is δ-correlated in time. This feature of the advecting field leads to a great theoretical simplification, not as much as to provide a closed-form theory for $\mathcal{S}_n$, but enough to allow a derivation of a differential equation for the simultaneous $2n$th-order correlation function $\mathcal{F}_{2n} = \langle \phi(\boldsymbol{r}_1) \ldots \phi(\boldsymbol{r}_{2n}) \rangle$, having the symbolic form [7]

$$\mathcal{O}\mathcal{F}_{2n} = RHS(\mathcal{F}_{2n-2}). \tag{6}$$

Guessing the scaling exponent of $\mathcal{F}_{2n}$ by power counting and balancing the LHS against the RHS yields dimensional scaling estimates which, in this case, are $\xi_{2n} = (2 - \zeta_2)n$. The crucial observation, however, is that the differential equation (6) possesses, in addition to the inhomogeneous solution that can be guessed by power counting, also homogeneous solutions

of the equation $\mathcal{O}\mathcal{F}_{2n} = 0$ [8–10]. These "zero modes" are homogeneous functions of their arguments but their exponent cannot be guessed from power counting; the scaling exponents are anomalous – i.e., $\xi_{2n} < (2-\zeta_2)n$ – and therefore dominant at small scales. As the scaling exponents appear in power-laws of the type $(r/\Lambda)^{\xi}$, Λ being some typical outer scale and $r \ll \Lambda$, the larger the exponent, the faster the decay of the contribution as the scale r diminishes. The exponents could be computed in perturbation theory around $\zeta_2 = 0$, demonstrating for the first time that dimensional scaling exponents are not the solution to the problem. For a further review see [11].

An appealing interpretation of the physical mechanism for anomalous exponents of the Kraichnan model was presented in the framework of the Lagrangian formulation [12]. In this formulation an nth-order correlation function results from averaging over all the Lagrangian trajectories of groups of n fluid points that started somewhere at $t = -\infty$ and ended their trajectories at points $\boldsymbol{r}_1 \dots \boldsymbol{r}_n$ at time $t = 0$. Analyzing this dynamics revealed that the Richardson diffusion of these groups did not contribute to anomalous scaling. Rather, it is the dynamics of the shapes (triangles for 3 points, tetrahedra for 4 points, etc.) that is responsible for the anomaly. In fact, the anomalous scaling exponents could be related to eigenvalues of operators made from the shape-to-shape transition probability [13]. The zero modes discussed above are *distributions over the space of shapes* that remain invariant to the dynamics [14]. It appears that these findings of the importance of shapes rather than scales in determining anomalous exponents is a new contribution to the plethora of anomalous exponents in field theory, and it would be surprising if other examples where shapes rather than scales are crucial will not appear in other corners of field theory, classical as well as quantum-mechanical.

The finding of distributions that remain invariant to the dynamics meant that there must be such distributions in the Eulerian frame as well, since the change from Lagrangian to Eulerian is just a smooth change of coordinates. Indeed this was the case; and this provided the clue to generalizing the results of the non-generic Kraichnan model to the generic case represented by Eq. (5) with a generic velocity field that stems from the Navier–Stokes equations. The central comment is that the decaying passive scalar problem, i.e. Eq. (5) with $f = 0$, is a linear problem for which one can always define a propagator from $\mathcal{F}_n$ at $t = 0$ (i.e. $\langle \phi(\boldsymbol{r}_1, t = 0) \cdots \phi(\boldsymbol{r}_n, t = 0) \rangle$) to the same object at time t (note that for the decaying problem this is no longer a stationary quantity) [15]. This propagator possesses eigenfunctions of eigenvalue 1 which are homogeneous functions of their arguments, characterized by anomalous exponents. They are the analogs of zero modes of the Kraichnan model, and are responsible for anomalous exponents in the generic case [16,17]. Thus the general statement that can be made is that the anomaly for the passive scalar, generic or otherwise, is due to the existence of "statistically preserved structures"; the structures can change in every single experiment, but remain invariant on the average. This is a novel notion that pertains to nonequilibrium systems without a known analog in equilibrium problems.

At present it is still unclear whether the insight gained from linear models might have direct relevance to the nonlinear velocity problem itself. Some positive indications in this direction can be found in [18], but much more needs to be done before firm conclusions can be drawn.

3. Statistical theory of anisotropic homogeneous turbulence

As mentioned above, the agents that produce turbulence tend to destroy its homogeneity and isotropy. In this section we are concerned about the loss of isotropy and review the extensive work that has been done to come to grips with this issue in a systematic fashion. Since this subject has been reviewed extensively [19], we limit this section to only a few essential comments.

The need for rethinking the issue of loss of isotropy was underlined by the appearance of several papers where anisotropic flows were analyzed disregarding anisotropy, and exponents were extracted from data assuming that the inertial range scales were isotropic. The results were confusing: scaling exponents varied from experiment to experiment, and from one position in the flow to another. If this were indeed the case, the notion of universality in turbulence would fail irreversibly. In fact, it can now be shown that all these worrisome results can be attributed to anisotropic contributions in the inertial range, as explained below.

The basic idea in dealing with anisotropy is that the equations of fluid mechanics are invariant to all rotations. Of course, these equations are also nonlinear, and therefore one cannot foliate them into the sectors of the SO(3) symmetry group. The equations for correlation functions are, however, linear (though forming an infinite hierarchy). Thus by expanding the correlation functions in the irreducible representations of the symmetry group, one gets a set of equations that are valid sector by sector [20]. The irreducible representations of the SO(3) symmetry group are organized by two quantum numbers j, m with $j = 0, 1, 2, \dots$ and $m = -j, -j+1, \dots j$. It turns out that the m components are mixed by the equations of motion, but the j components are not. Accordingly one can show that an n-point correlation function admits the expansion

$$\boldsymbol{F}_n(\boldsymbol{r}_1, \boldsymbol{r}_2, \dots \boldsymbol{r}_n) = \sum_{qjm} A_{qjm}(r_1, r_2, \dots, r_n) \times \boldsymbol{B}_{qjm}(\hat{\mathbf{r}}_1, \hat{\mathbf{r}}_2 \dots \hat{\mathbf{r}}_n), \tag{7}$$

where $\hat{\mathbf{r}}$ is a unit vector in the direction of $\boldsymbol{r}$, and A_{qjm} is a homogeneous function of the scalar $r_1 \dots r_n$,

$$A_{qjm}(\lambda r_1, \lambda r_2, \dots, \lambda r_n) = \lambda^{\zeta_n^{(j)}} A_{qjm}(r_1, r_2, \dots, r_n). \tag{8}$$

Here $\zeta_n^{(j)}$ is the scaling exponent characterizing the j-sector of the symmetry group for the nth-order correlation function. $\boldsymbol{B}_{qjm}(\hat{\mathbf{r}}_1, \hat{\mathbf{r}}_2 \dots \hat{\mathbf{r}}_n)$ are the n-rank tensorial irreducible representations of the SO(3) symmetry group, and the index q in Eq. (7) is due to the fact that higher-order tensors have more than one irreducible representation with the same j, m [20].

It was shown that this property of the nth-order correlation functions is inherited by the structure functions as well [21]. Since these are scalar functions of a vector argument they get expanded in standard spherical harmonics $\phi_{jm}(\hat{\mathbf{R}})$

$$S_n(\boldsymbol{R}) = \sum_{jm} a_{jm}(r)\phi_{jm}(\hat{\mathbf{R}}), \tag{9}$$

with

$$a_{jm}(\lambda r) = \lambda^{\zeta_n^{(j)}} a_{jm}(r). \tag{10}$$

The main issue for research was the numerical values of this plethora of scaling exponents.

Of considerable help in organizing the scaling exponents in the various sectors of the symmetry group were the Kraichnan model and related models (like the passive vector model with pressure), where the exponents could be computed analytically in the Eulerian frame in any sector of the symmetry group. The central quantitative result of the Eulerian calculation is the expression for the scaling exponent $\xi_j^{(n)}$ which is associated with the scaling behavior of the nth-order correlation function (or structure function) of the scalar field in the jth sector of the symmetry group. In other words, this is the scaling exponent of the projection of the correlation function on the jth irreducible representation of the SO(d) symmetry group, d being the space dimension, with n and j taking on even values only, $n = 0, 2, \ldots$ and $j = 0, 2, \ldots$ [23]:

$$\xi_j^{(n)} = n - \epsilon\left[\frac{n(n+d)}{2(d+2)} - \frac{(d+1)j(j+d-2)}{2(d+2)(d-1)}\right] + O(\epsilon^2). \tag{11}$$

The result is valid for any even $j \le n$, and to $O(\epsilon)$. In the isotropic sector ($j = 0$) we recover the result of [8]. It is noteworthy that for higher values of j the discrete spectrum is a strictly increasing function of j. This is important, since it shows that for diminishing scales the higher-order scaling exponents become irrelevant, and for sufficiently small scales only the isotropic contribution survives. Recall that the scaling exponents appear in power-laws of the type $(r/\Lambda)^{\xi}$ with Λ a typical outer scale and $r \ll \Lambda$; the larger the exponent, the faster the decay of the contribution as the scale r diminishes. This is precisely how the isotropization of small scales takes place, with the higher-order exponents describing the rate of isotropization. Nevertheless, for intermediate scales or for finite values of the Reynolds and Peclet numbers, the lower-lying scaling exponents will appear in all the measured quantities, and understanding their role and disentangling their various contributions cannot be avoided.

For Navier–Stokes turbulence the exponents cannot be computed analytically, but the results obtained from experiments [21] and simulations [22] indicate that the picture obtained for the Kraichnan model repeats itself. The isotropic sector is always leading (in the sense that scaling exponents belonging to higher sector are numerically larger). There is growing evidence of universality of scaling exponents in all the sectors, but this issue is far from being settled, and more experiments and simulations are necessary to provide decisive evidence. It is noteworthy that the issue of universality of the exponents in the isotropic sector is here expanded many-fold into all the sectors of the symmetry group, and is certainly worth further study.

4. Wall-bounded turbulence

Turbulent flows of highest relevance for engineering application possess neither isotropy nor homogeneity. For example, turbulent flows in channels and pipes are strongly anisotropic and inhomogeneous; indeed, in a stationary plane channel flow with a constant pressure gradient $p' \equiv -\mathrm{d}p/\mathrm{d}x$ the only component of the mean velocity $\boldsymbol{V}$, the streamwise component $V_x \equiv V$, depends strongly on the wall normal direction z; the derivatives of V_x with respect to z and the second-order quantities such as mean-square-fluctuations similarly depend only on z. A long-standing challenge is the description of the **profiles** of the mean velocity and second-order fluctuations throughout the channel or pipe at relatively high but finite Reynolds numbers.

To understand the issue, focus on a channel of width $2L$ between its parallel walls, where the incompressible fluid velocity $\boldsymbol{U}(\boldsymbol{r}, t)$ is decomposed into its mean (i.e., average over time) and a fluctuating part

$$\boldsymbol{U}(\boldsymbol{r}, t) = \boldsymbol{V}(\boldsymbol{r}) + \boldsymbol{u}(\boldsymbol{r}, t), \quad \boldsymbol{V}(\boldsymbol{r}) \equiv \langle \boldsymbol{U}(\boldsymbol{r}, t)\rangle. \tag{12}$$

Near the wall, the mean velocity profiles for different Reynolds numbers exhibit data collapse once presented in wall units. Here in "data collapse" we mean that data obtained at different experimental conditions can be collapsed on the same curve by re-plotting in different units (see Fig. 4 for example). The 'wall units' are obtained by defining the Reynolds number Re_τ, the normalized distance from the wall z^+ and the normalized mean velocity $V^+(z^+)$ (for channels) by

$$Re_\tau \equiv L\sqrt{p'L}/\nu, \qquad z^+ \equiv zRe_\tau/L, \qquad V^+ \equiv V/\sqrt{p'L}.$$

The classical theory of Prandtl and von Kármán for infinitely large Re_τ is based on dimensional reasoning and on the assumption that *the single characteristic scale in the problem is proportional to the distance from the (nearest) wall* (see below for details). It leads to the celebrated von Kármán log-law [1]

$$V^+(z^+) = \kappa^{-1}\ln(z^+) + B\,, \tag{13}$$

which serves as a basis for the parametrization of turbulent flows near a wall in many engineering applications. On the face of it, this law agrees with the data (see, e.g. Fig. 1) for relatively large z^+, say for $z^+ > 100$, giving $\kappa \sim 0.4$ and $B \sim 5$. The range of validly of the log-law is definitely restricted by the requirement $\zeta \ll 1$, where $\zeta \equiv z/L$ (channel) or $\zeta \equiv r/R$ (pipe of radius R). For $\zeta \sim 1$ the global geometry becomes important leading to unavoidable deviations of $V^+(\zeta)$ from the log-law (13), known as *the wake*.

The problem is that for finite Re_τ the corrections to the log-law (13) are in powers of $\varepsilon \equiv 1/\ln Re_\tau$ [24,25] and definitely cannot be neglected for the currently largest available direct numerical simulation (DNS) of channel flows ($Re_\tau = 2003$ [26,27] or $\varepsilon \approx 0.13$). Even for Re_τ approaching 500,000

as in the Princeton superpipe experiment [28], $\varepsilon \approx 0.08$. This opens a Pandora box with various possibilities to revise the log-law (13) and to replace it, as was suggested in [24], by a power-law

$$V^+(z^+) = C(Re_\tau)(z^+)^{\gamma(Re_\tau)} . \tag{14}$$

Here both the coefficients $C(Re_\tau)$ and the exponents $\gamma(Re_\tau)$ were represented as asymptotic series expansions in ε. The relative complexity of this proposition compared to the simplicity of Eq. (13) resulted in a mixed response in the fluid mechanics community [29], leading to a controversy. Various attempts [24,28–32] to validate the log-law (13) or the alternative power-law (14) were based on extensive analysis of experimental data used to fit the velocity profiles as a formal expansion in inverse powers of ε or as composite expansions in both z^+ and ζ.

Recently a complementary approach to this issue was proposed on the basis of experience with critical phenomena where one employs scaling functions rather than scaling laws [33]. The essence of this approach is the realization that a characteristic scale, say $\widetilde{\ell}$, may depend on the position in the flow. The simple scaling assumption near the wall, $\widetilde{\ell}^+ = \kappa z^+$, leads to the log-law (13). The alternative suggestion of [24], $\widetilde{\ell}^+ \propto (z^+)^{\alpha(Re_\tau)}$, leads to alternative power-law (14). But there is no physical reason why $\widetilde{\ell}$ should behave in either manner. Instead, it was shown that $\widetilde{\ell}/L$ should depend on $\zeta = z/L$, approaching $\kappa\zeta$ in the limit $\zeta \to 0$ (in accordance with the classical thinking). However, for $\zeta \sim 1$, $\widetilde{\ell}$ should saturate at some level below κL due to the effect of the other wall. We recall now the recent analysis of DNS data that provides a strong support to this idea, allowing one to get, within the traditional (second-order) closure procedure, a quantitative description of the following three quantities: the mean shear, $S(z) = \mathrm{d}V(z)/\mathrm{d}z$, the kinetic energy density (per unit mass), $K(z) \equiv \langle |\boldsymbol{u}|^2\rangle/2$, and the tangential Reynolds stress, $W(z) \equiv -\langle u_x u_z\rangle$. This is achieved in the entire flow and in a wide region of Re_τ, using only three Re_τ-independent parameters.

The first relation between these objects follows from the Navier–Stokes equation for the mean velocity. The resulting equation is exact, being the mechanical balance between the momentum generated at distance z from the wall, i.e. $p'(L - z)$, and the momentum transferred to the wall by kinematic viscosity and turbulent transport. In physical and wall units it has the form

$$\nu S + W = p'(L - z) \Rightarrow S^+ + W^+ = 1 - \zeta. \tag{15}$$

Neglecting the turbulent diffusion of energy (known to be relatively small in the log-law region), one gets a second relation as a local balance between the turbulent energy generated by the mean flow at a rate SW, and the dissipation at a rate $\varepsilon_K \equiv \nu\langle|\nabla u|^2\rangle$: $\varepsilon_K \approx SW$. For stationary conditions ε_K equals the energy flux toward smaller scales from the outer scale of turbulence, $\widetilde{\ell}_K$. Thus, the flux is estimated as $\gamma_K(z)K(z)$, where $\gamma_K(z)$ is the typical eddy turnover inverse time, estimated as $\sqrt{K(z)}/\widetilde{\ell}_K(z)$. This gives rise to the other (now approximate) relations:

$$S^+W^+ \approx \varepsilon_K^+, \quad \varepsilon_K^+ = \gamma_K^+ K^+ = K^+\sqrt{K^+}/\widetilde{\ell}_K^+. \tag{16}$$

The third required relationship can be obtained from the Navier Stokes equation, similar to Eq. (16), as the local balance between the rate of Reynolds stress production $\approx SK$ and its dissipation ε_W: $\varepsilon_W \approx SK$. The main contribution to ε_W comes from the so-called Return-to-Isotropy process and can be estimated [34], similarly to ε_K, as $\gamma_W W$ with $\gamma_W = \sqrt{K}/\widetilde{\ell}_W$, involving yet another length scale $\widetilde{\ell}_W$ which is of the same order of magnitude as ℓ_K. Thus one has, similarly to Eq. (16),

$$S^+K^+ \approx \varepsilon_W^+, \qquad \varepsilon_W^+ = \gamma_W^+ W^+ = W^+\sqrt{K^+}/\widetilde{\ell}_W^+. \tag{17}$$

Now we show that the source of ambiguity is the assumption that the length scales can be determined *a priori* as $\ell_{K,W}^+ \propto (z^+)^\alpha$ with $\alpha = 1$ or $\alpha \neq 1$. In reality we have another characteristic length scale, i.e. L, that also should enter the picture when $\zeta = z/L$ is not very small. The actual dependence $\widetilde{\ell}_W$ and $\widetilde{\ell}_K$ on z and L can be found from the data. Consider first $\widetilde{\ell}_W$, defined by Eq. (17), and introduce a new scale $\ell_W \equiv \widetilde{\ell}_W r_W(z^+)/\kappa_W$ such that

$$\ell_W^+ \equiv \frac{W^+(z^+, Re_\tau)\, r_W(z^+)}{\kappa_W S^+(z^+, Re_\tau)\sqrt{K^+(z^+, Re_\tau)}} . \tag{18}$$

Here, $r_W(z^+)$ is a universal i.e. Re_τ-independent dimensionless *function* of z^+, chosen such that new scale $\ell_W/L = \ell_W^+/Re_\tau$ becomes a Re_τ-independent function of only one variable $\zeta = (z/L) = (z^+/Re_\tau)$. The dimensionless constant $\kappa_W \approx 0.20$ is chosen to ensure that $\lim_{z\ll L} \ell_W^+(\zeta) = z^+$. Note that if r_W were a constant, ℓ_W would have started near the wall quadratically, i.e. as $z \times z^+$. Later ℓ_W^+ would have become $\propto z^+$ for $50 \ll z^+ \ll Re_\tau$ [34]. Thus to normalize it to slope 1 we need the function $r_W(z^+)$ that behaves as $1/z^+$ for $z^+ \ll 50$ and approaches unity (under a proper choice of κ_W) for $z^+ \gg 50$. A choice that leads to good data collapse is

$$r_W(z^+) = \left[1 + \left(\ell_{\mathrm{buf}}^+/z^+\right)^6\right]^{1/6}, \quad \ell_{\mathrm{buf}}^+ \approx 49, \tag{19}$$

where ℓ_{buf}^+ is a Re_τ-independent length that plays a role of the crossover scale (in wall units) between the buffer and log regions. The quality of the data collapse for this scaling function is demonstrated in Fig. 2.

The second length scale, $\widetilde{\ell}_K^+$, is determined by Eq. (16):

$$\widetilde{\ell}_K^+ \equiv \frac{(K^+(z^+, Re_\tau))^{3/2}}{\varepsilon_K^+(z^+, Re_\tau)} = \kappa_K \ell_K^+, \quad \kappa_K \approx 3.7. \tag{20}$$

In Fig. 2 we demonstrate that this simple scaling function leads to good data collapse everywhere except perhaps in the viscous layer. We will see below that this has only negligible effects on our results.

Solution and velocity profiles: Solving Eqs. (16) and (17) and accounting for Eqs. (18) and (20) we find

$$W^+ = \left(\kappa S^+ \ell^+\right)^2 r_W^{-3/2}, \tag{21}$$

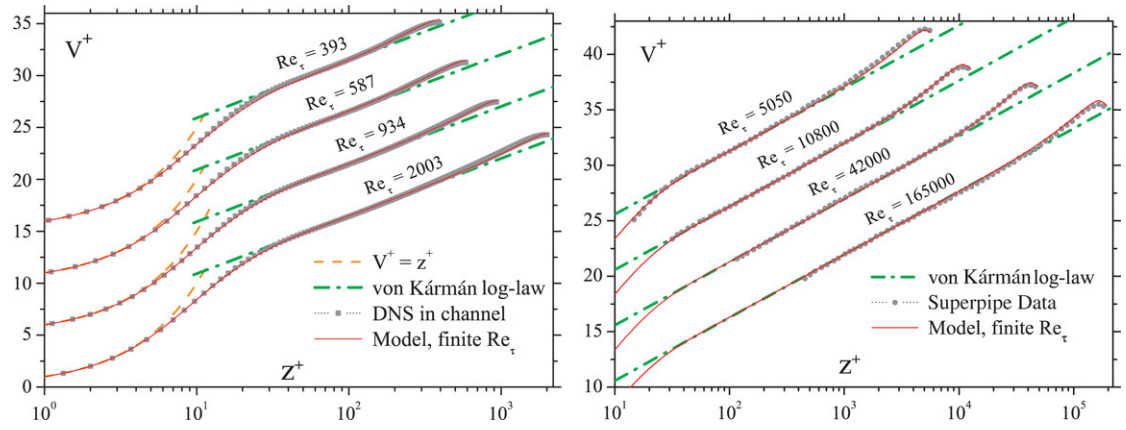

Fig. 1. Color online. Comparison of the theoretical mean velocity profiles (red solid lines) at different values of Re_τ with the DNS data for the channel flow [26,27] (left panel, grey squares; model with $\ell_{\rm buf} = 49$, $\kappa = 0.415$, $\ell_s = 0.311$) and with the experimental superpipe data [28] (right panel, grey circles; model with $\ell_{\rm buf} = 46$, $\kappa = 0.405$, $\ell_s = 0.275$). In orange dashed line we plot the viscous solution $V^+ = z^+$. In green dashed dotted line we present the von Kármán log-law. Note that the theoretical predictions with three Re_τ-independent parameters fits the data throughout the channel and pipe, from the viscous scale, through the buffer layer, the log-layer and the wake. For clarity different plots are shifted vertically by five units.

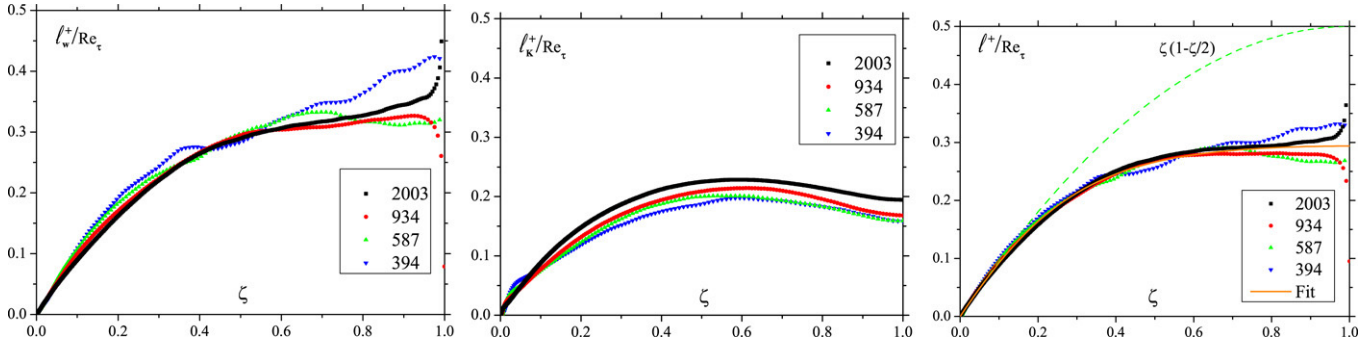

Fig. 2. Color online. The scaling function $\ell_W^+(\zeta)/Re_\tau$ (left panel), $\ell_K^+(\zeta)/Re_\tau$ (middle panel) and the final scaling function $\ell^+(\zeta)$ (right panel), as a function of $\zeta \equiv z/L$, for four different values of Re_τ, computed from the DNS data [26,27]. Note that the data collapse everywhere except at $\zeta \to 1$ where $W^+ \sim S^+ \ll 1$ and accuracy is lost. The green dash line represents $\widetilde{\zeta} = \zeta\,(1 - \zeta/2)$ with a saturation level 0.5; in orange solid line we show the fitted function Eq. (24) with $\ell_{\rm sat} = 0.311$.

where we have defined the von Kármán constant and the crucial scaling function $\ell^+(\zeta)$ as

$$\kappa \equiv (\kappa_W^3 \kappa_K)^{1/4} \approx 0.415, \qquad \ell^+ \equiv [{\ell_W^+}^3(\zeta)\,\ell_K^+(\zeta)]^{1/4}. \quad (22)$$

The convincing data collapse for the resulting function $\ell^+(\zeta)/Re_\tau$ is shown in Fig. 2, rightmost panel. Substituting Eq. (21) in Eq. (15) we find a quadratic equation for S with the solution

$$S^+ = \frac{\sqrt{1 + (1-\zeta)[2\kappa\ell^+(\zeta)]^2/r_W(z^+)^{3/2}} - 1}{2[\kappa\ell^+(\zeta)]^2/r_W(z^+)^{3/2}}. \quad (23)$$

To integrate this equation and find the mean velocity profile for any value of Re_τ we need to determine the scaling function $\ell^+(\zeta)$ from the data. A careful analysis of the DNS data allows us to find a good *one-parameter* fit for $\ell^+(\zeta)$,

$$\frac{\ell^+(\zeta)}{Re_\tau} = \ell_s \left\{1 - \exp\left[-\frac{\widetilde{\zeta}}{\ell_s}\left(1 + \frac{\widetilde{\zeta}}{2\ell_s}\right)\right]\right\}, \quad (24)$$

where $\widetilde{\zeta} \equiv \zeta(1 - \zeta/2)$ and $\ell_s \approx 0.311$. The quality of the fit is obvious from the continuous line in the rightmost panel of Fig. 2.

Finally the theory for the mean velocity contains three parameters, namely ℓ_s together with $\ell^+_{\rm buff}$ and κ. We demonstrate now that with these three parameters we can determine the mean velocity profile for any value Re_τ, throughout the channel, including the viscous layer, the buffer layer, the log-law region and the wake. Examples of the integration of Eq. (23) are shown in Fig. 1. We trust that, irrespective of the reader's own preference to the log-law or the power-law, he would agree that these fits are very good. It remains now to estimate, using (23), the conditions under which we expect to see a log-law and those when deviations due to finite Re_τ would seem important. In addition, our theory yields the kinetic energy and Reynolds stress profiles which are in qualitative agreement with the DNS data; for W profiles see Fig. 3.

To show that the present approach is quite general, we apply it now to the experimental data that were at the center of the controversy [24], i.e., the Princeton superpipe data [28]. In Fig. 1 right panel we show the mean velocity profiles measured in the superpipe compared with our prediction using *the same scaling function* $\ell^+(\zeta)$. Note that the data spans values of Re_τ from 5050 to 165,000, and the fits with only three Re_τ-

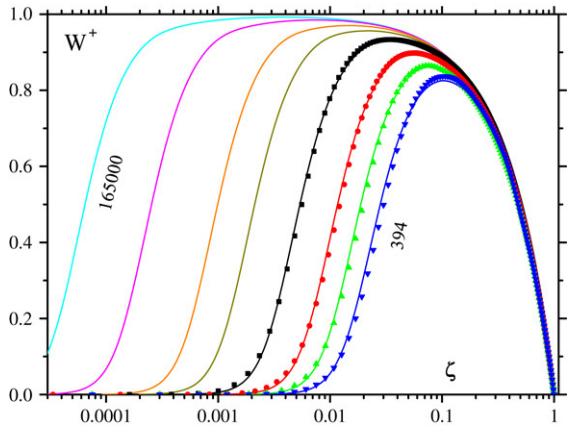

Fig. 3. The Reynolds stress profiles (solid lines) at Re_τ from 394 to 2003 (in channel) and from 5050 to 165,000 (in pipe) in comparison with available DNS data (dots) for the channel.

independent constants are excellent. Note the 2% difference in the value of κ between the DNS and the experimental data; we do not know at this point whether this stems from inaccuracies in the DNS or the experimental data, or whether turbulent flows in different geometries have different values of κ. While the latter is theoretically questionable, we cannot exclude this possibility until a better understanding of how to compute κ from first principles is achieved.

So far we discussed turbulent channel and pipe flows and demonstrated the existence and usefulness of a scaling function $\ell^+(\zeta)$ which allows us to get the profiles of the mean velocities for all values of Re_τ and throughout the channel. While this function begins near the wall as z^+, it saturates later, and its full functional dependence on ζ is crucial for finding the correct mean velocity profiles. The approach also allows us to delineate the accuracy of the log-law presentation, which depends on z^+ and the value of Re_τ. For asymptotically large Re_τ the region of the log-law can be very large, but nevertheless it breaks down near the mid channel and near the buffer layer, where corrections were presented.

The future challenge is to apply this idea to other examples of wall-bounded flows, including time-developing boundary layers, turbulent flows with temperature gradients or laden with particles. There may be more typical "lengths" in such systems, and it is very likely that turning these lengths into scaling functions will provide new insights and better models for a variety of engineering applications. Such efforts are not entirely new; see, for example, [35].

5. Drag reduction by additives

One severe technological problem with turbulent flows is that they cost a lot to maintain; the drag that the fluid exerts on the wall increases significantly when turbulence sets in. It is therefore important that there exist additives, in particular polymers and bubbles, that can reduce this drag significantly. Over the last few years there has been great progress in understanding these phenomena, and here we provide a short review of this progress.

5.1. Drag reduction by polymers

The addition of few tens of parts per million (by weight) of long-chain polymers to turbulent fluid flows in channels or pipes can bring about a reduction of the friction drag by up to 80% [36–39]. This phenomenon of "drag reduction" is well documented and is used in technological applications from fire engines (allowing a water jet to reach high floors) to oil pipes. In spite of a large amount of experimental and simulations data, the fundamental mechanism for drag reduction has remained under debate for a long time [39–41]. In such wall-bounded turbulence, the drag is caused by momentum dissipation at the walls. For Newtonian flows (in which the kinematic viscosity is constant) the momentum flux is dominated by the so-called Reynolds stress, leading to the logarithmic (von-Kármán) dependence of the mean velocity on the distance from the wall [34]. However, with polymers, the drag reduction entails a change in the von-Kármán log-law such that a much higher mean velocity is achieved. In particular, for high concentrations of polymers, a regime of maximum drag reduction is attained (the "MDR asymptote"), independent of the chemical identity of the polymer [37], see Fig. 4. During the last few years the fundamental mechanism for this phenomenon was elucidated: while momentum is produced at a fixed rate by the forcing, polymer stretching results in a suppression of the momentum flux from the bulk to the wall. Accordingly the mean velocity in the channel must increase. It was shown that polymer stretching results in an effective viscosity that increases linearly with the distance from the wall. The MDR asymptote is consistent with the largest possible such linear increase in viscosity for which turbulent solutions still exist. In other words, the MDR is an edge solution separating turbulent from laminar flows. This insight allowed one to derive the MDR as a new logarithmic law for the mean velocity with a slope that fits existing numerical and experimental data. The law is universal, explaining the MDR asymptote.

5.2. Short review of the theory

The riddle of drag reduction can be introduced by a juxtaposition of the effect of polymers with respect to the universal Newtonian law (13). In the presence of long chain polymers the mean velocity profile $V^+(y^+)$ (for a fixed value of p' and channel geometry) changes dramatically. For sufficiently large concentration of polymers $V^+(y^+)$ saturates to a new (universal, polymer independent) "law of the wall" [37],

$$V^+(y^+) = {\kappa_{\rm V}}^{-1} \ln\left(e\,\kappa_{\rm V}\, y^+\right) \quad \text{for } y^+ \gtrsim 10. \tag{25}$$

This law, which was discovered experimentally by Virk (and hence the notation $\kappa_{\rm V}$), is also claimed to be universal, independent of the Newtonian fluid and the nature of the polymer additive, including flexible and rigid polymers [38]. Previous to our work in this network, the numerical value of the coefficient $\kappa_{\rm V}$ was known only from experiments, ${\kappa_{\rm V}}^{-1} \approx 11.7$, giving a phenomenological MDR law in the form [37]

$$V^+(y^+) = 11.7 \ln y^+ - 17. \tag{26}$$

For smaller concentration of polymers the situation is as shown in Fig. 4. The Newtonian law of the wall (13) is the black solid line for $y^+ \gtrsim 30$. The MDR asymptote (25) is the dashed red line. For intermediate concentrations the mean velocity profile starts along the asymptotic law (25), and then crosses over to the so-called "Newtonian plug" with a Newtonian logarithmic slope identical to the inverse of von-Kármán's constant. The region of values of y^+ in which the asymptotic law (25) prevails was termed "the elastic sublayer" [37]. The relative increase of the mean velocity (for a given p') due to the existence of the new law of the wall (25) *is* the phenomenon of drag reduction. Thus the main theoretical challenge is to understand the origin of the new law (25), and in particular its universality, or independence of the polymer used. A secondary challenge is to understand the concentration-dependent cross over back to the Newtonian plug. In our work we argue that the phenomenon can be understood mainly by the influence of the polymer stretching on the y^+-dependent effective viscosity. The latter becomes a crucial agent in carrying the momentum flux from the bulk of the channel to the walls (where the momentum is dissipated by friction). In the Newtonian case the viscosity has a negligible role in carrying the momentum flux; this difference gives rise to the change of Eq. (13) in favor of Eq. (25) which we derive below.

The equations of motion of polymer solutions are written in the FENE-P approximation [42,43] by coupling the fluid velocity $\boldsymbol{u}(\boldsymbol{r}, t)$ to the tensor field of "polymer conformation tensor" $\boldsymbol{R}(\boldsymbol{r}, t)$. The latter is made from the "end-to-end" separation vector as $R_{\alpha\beta}(\boldsymbol{r}, t) \equiv \langle r_\alpha r_\beta \rangle$, and it satisfies the equation of motion

$$\frac{\partial R_{\alpha\beta}}{\partial t} + (u_\gamma \nabla_\gamma) R_{\alpha\beta} = \frac{\partial u_\alpha}{\partial r_\gamma} R_{\gamma\beta} + R_{\alpha\gamma} \frac{\partial u_\beta}{\partial r_\gamma} - \frac{1}{\tau}\left[P(\boldsymbol{r}, t) R_{\alpha\beta} - \rho_0^2 \delta_{\alpha\beta}\right],$$

$$P(\boldsymbol{r}, t) = (\rho_m^2 - \rho_0^2)/(\rho_m^2 - R_{\gamma\gamma}) \tag{27}$$

ρ_m^2 and ρ_0^2 refer to the maximal and the equilibrium values of the trace $R_{\gamma\gamma}$. In most applications $\rho_m \gg \rho_0$

$$P(r, t) \approx (1/(1 - \alpha R_{\gamma\gamma})),$$

where $\alpha = \rho_m^{-2}$. The equation for the fluid velocity field gains a new stress tensor:

$$\frac{\partial u_\alpha}{\partial t} + (u_\gamma \nabla_\gamma) u_\alpha = -\nabla_\alpha p + \nu_s \nabla^2 u_\alpha + \nabla_\gamma T_{\alpha\gamma} \tag{28}$$

$$T_{\alpha\beta}(r, t) = \frac{\nu_p}{\tau}\left[\frac{P(r, t)}{\rho_0^2} R_{\alpha\beta}(r, t) - \delta_{\alpha\beta}\right]. \tag{29}$$

Here ν_s is the viscosity of the neat fluid, and ν_p is a viscosity parameter which is related to the concentration of the polymer, i.e. $\nu_p/\nu_s \sim c_p$.

We shall use the approximation

$$T_{\alpha\beta} \sim \frac{\nu_p}{\tau} \frac{P}{\rho_0^2} R_{\alpha\beta}.$$

Armed with the equation for the viscoelastic medium we establish the mechanism of drag reduction following the standard strategy of Reynolds. Eq. (15) changes now to another exact relation [44] between the objects S and W which includes the effect of the polymers:

$$W + \nu S + \frac{\nu_p}{\tau} \langle P R_{xy} \rangle(y) = p'(L - y). \tag{30}$$

On the RHS of this equation we see the production of momentum flux due to the pressure gradient; on the LHS we have the Reynolds stress, the Newtonian viscous contribution to the momentum flux, and the polymer contribution to the momentum flux. A second relation between $S(y)$, $W(y)$, $K(y)$ and $\boldsymbol{R}(y)$ is obtained from the energy balance. In Newtonian fluids the energy is created by the large scale motions at a rate of $W(y)S(y)$. It is cascaded down the scales by a flux of energy, and is finally dissipated at a rate ϵ, where $\epsilon = \nu \langle |\nabla u|^2 \rangle$. In viscoelastic flows one has an additional contribution due to the polymers. Our calculation [44] showed that the energy balance equation takes the form:

$$a\nu \frac{K}{y^2} + b \frac{K^{3/2}}{y} + \frac{A^2 \nu_p}{2\tau^2} \langle P \rangle^2 (\langle R_{yy} \rangle + \langle R_{zz} \rangle) = WS. \tag{31}$$

We note that contrary to Eq. (30) which is exact, Eq. (31) is not exact. We expect it, however, to yield good order of magnitude estimates as is demonstrated below. Finally, we quote the experimental fact [37] that outside the viscous boundary layer

$$\frac{W(y)}{K(y)} = \begin{cases} c_{\mathrm{N}}^2, & \text{for Newtonian flow,} \\ c_{\mathrm{V}}^2, & \text{for viscoelastic flow.} \end{cases} \tag{32}$$

The coefficients c_{N} and c_{V} are bounded from above by unity. (The proof is $|c| \equiv |W|/K \le 2|\langle u_x u_y \rangle|/\langle u_x^2 + u_y^2 \rangle \le 1$, because $(u_x \pm u_y)^2 \ge 0$.)

To proceed, one needs to estimate the various components of the polymer conformation tensor. This was done in [45] with the final result that for c_p large (where $P \approx 1$), and Deborah number $\mathrm{De} \equiv \tau S(y) \gg 1$ the conformation tensor is highly anisotropic,

$$\boldsymbol{R}(y) \simeq R^{yy}(y) \begin{pmatrix} 2\mathrm{De}^2(y) & \mathrm{De}(y) & 0 \\ \mathrm{De}(y) & 1 & 0 \\ 0 & 0 & C(y) \end{pmatrix}.$$

The important conclusion is that the term proportional to $\langle R_{yy} \rangle$ in Eq. (31) can be written as $\nu_p \langle \mathcal{R}_{yy} \rangle(y) S(y)$. Defining the "effective viscosity" $\nu(y)$ according to

$$\nu(y) = \nu_0 + \nu_p \langle \mathcal{R}_{yy} \rangle(y). \tag{33}$$

The momentum balance equation attains the form

$$\nu(y) S(y) + W(y) = p' L. \tag{34}$$

It was shown in [44] that also the energy balance equation can be rewritten with the very same effective viscosity, i.e.,

$$\nu(y) \left(\frac{a}{y}\right)^2 K(y) + \frac{b\sqrt{K(y)}}{y} K(y) = W(y) S(y). \tag{35}$$

In the MDR region the first term on the RHS in Eqs. (34) and (35) dominate; from the first equation $\nu(y) \sim 1/S(y)$. Put

in Eq. (35) this leads to $S(y) \sim 1/y$, which translates to the new logarithmic law which is the MDR. We will determine the actual slope momentarily. At this point one needs to stress that this results means that $\nu(y)$ must be proportional to y in the MDR regime. This linear dependence of the effective viscosity is one of the central discoveries of our approach. Translated back, it predicts that $\langle R_{yy}\rangle \sim y$ outside the boundary layer. This prediction is well supported by numerical simulations.

The crucial new insight that explained the universality of the MDR and furnished the basis for its calculation is that the MDR is a marginal flow state of wall-bounded turbulence: attempting to increase $S(y)$ beyond the MDR results in the collapse of the turbulent solutions in favor of a stable laminar solution $W = 0$. As such, the MDR is universal by definition, and the only question is whether a polymeric (or other additive) can supply the particular effective viscosity $\nu(y)$ that drives Eqs. (34) and (35) to attain the marginal solution that maximizes the velocity profile. We predict that the same marginal state will exist in numerical solutions of the Navier–Stokes equations furnished with a y-dependent viscosity $\nu(y)$. There will be no turbulent solutions with velocity profiles higher than the MDR.

To see this explicitly, we first rewrite the balance equations in wall units. For constant viscosity (i.e. $\nu(y) \equiv \nu_0$), Eqs. (34) and (35) form a closed set of equations for $S^+ \equiv S\nu_0/(P'L)$ and $W^+ \equiv W/\sqrt{P'L}$ in terms of two dimensionless constant $\delta^+ \equiv a\sqrt{K/W}$ (the thickness of the viscous boundary layer) and $\kappa_K \equiv b/c_V^3$ (the von Kármán constant). Newtonian experiments and simulations agree well with a fit using $\delta^+ \sim 6$ and $\kappa_K \sim 0.436$ (see the black continuous line in Fig. 4 which shows the mean velocity profile using these very constants). Once the effective viscosity $\nu(y)$ is no longer constant we expect c_V to change and consequently the two dimensionless constants will change as well. We will denote the new constants as Δ and κ_C respectively. Clearly one must require that for $\nu(y)/\nu_0 \to 1$, $\Delta \to \delta^+$ and $\kappa_C \to \kappa_K$. The balance equations are now written as

$$\nu^+(y^+)S^+(y^+) + W^+(y^+) = 1, \tag{36}$$

$$\nu^+(y^+)\frac{\Delta^2}{y^{+2}} + \frac{\sqrt{W^+}}{\kappa_C y^+} = S^+. \tag{37}$$

where $\nu^+(y^+) \equiv \nu(y^+)/\nu_0$. Substituting now S^+ from Eq. (36) into Eq. (37) leads to a quadratic equation for $\sqrt{W^+}$. This equation has as a zero solution for W^+ (laminar solution) as long as $\nu^+(y^+)\Delta/y^+ = 1$. Turbulent solutions are possible only when $\nu^+(y^+)\Delta/y^+ < 1$. Thus at the edge of existence of turbulent solutions we find $\nu^+ \propto y^+$ for $y^+ \gg 1$. This is not surprising, since it was observed already in previous work that the MDR solution is consistent with an effective viscosity which is asymptotically linear in y^+ [46,47]. It is therefore sufficient to seek the edge solution of the velocity profile with respect to linear viscosity profiles, and we rewrite Eqs. (36) and (37) with an effective viscosity that depends linearly on y^+ outside the boundary layer of thickness δ^+:

$$[1 + \alpha(y^+ - \delta^+)]S^+ + W^+ = 1\,, \tag{38}$$

$$[1 + \alpha(y^+ - \delta^+)]\frac{\Delta^2(\alpha)}{y^{+2}} + \frac{\sqrt{W^+}}{\kappa_C y^+} = S^+\,. \tag{39}$$

We now endow Δ with an explicit dependence on the slope of the effective viscosity $\nu^+(y)$, $\Delta = \Delta(\alpha)$. Since drag reduction must involve a decrease in W, we expect the ratio a^2K/W to depend on α, with the constraint that $\Delta(\alpha) \to \delta^+$ when $\alpha \to 0$. Although Δ, δ^+ and α are all dimensionless quantities, physically Δ and δ^+ represent (viscous) length scales (for the linear viscosity profile and for the Newtonian case, respectively) while α^{-1} is the scale associated to the slope of the linear viscosity profile. It follows that $\alpha\delta^+$ is dimensionless even in the original physical units. It is thus natural to present $\Delta(\alpha)$ in terms of a dimensionless scaling function $f(x)$,

$$\Delta(\alpha) = \delta^+ f(\alpha\delta^+). \tag{40}$$

Obviously, $f(0) = 1$. In [48] it was shown that the balance equations (38) and (39) (with the prescribed form of the effective viscosity profile) have a nontrivial symmetry that leaves them invariant under rescaling of the wall units. This symmetry dictates the function $\Delta(\alpha)$ in the form

$$\Delta(\alpha) = \frac{\delta^+}{1 - \alpha\delta^+}. \tag{41}$$

Armed with this knowledge we can now find the maximal possible velocity far away from the wall, $y^+ \gg \delta^+$. There the balance equations simplify to

$$\alpha y^+ S^+ + W^+ = 1, \tag{42}$$

$$\alpha\Delta^2(\alpha) + \sqrt{W^+}/\kappa_C = y^+S^+. \tag{43}$$

These equations have the y^+-independent solution for $\sqrt{W^+}$ and y^+S^+:

$$\sqrt{W^+} = -\frac{\alpha}{2\kappa_C} + \sqrt{\left(\frac{\alpha}{2\kappa_C}\right)^2 + 1 - \alpha^2\Delta^2(\alpha)},$$

$$y^+S^+ = \alpha\Delta^2(\alpha) + \sqrt{W^+}/\kappa_C. \tag{44}$$

By using Eq. (44) (see Fig. 5), we obtain that the edge solution ($W^+ \to 0$) corresponds to the supremum of y^+S^+, which happens precisely when $\alpha = 1/\Delta(\alpha)$. Using Eq. (41) we find the solution $\alpha = \alpha_m = 1/2\delta^+$. Then $y^+S^+ = \Delta(\alpha_m)$, giving $\kappa_V^{-1} = 2\delta^+$. Using the estimate $\delta^+ \approx 6$ we get the final prediction for the MDR. Using Eq. (25) with $\kappa_V^{-1} = 12$, we get

$$V^+(y^+) \approx 12\ln y^+ - 17.8. \tag{45}$$

This result is in close agreement with the empirical law (26) proposed by Virk. The value of the intercept on the RHS of Eq. (45) follows from Eq. (25) which is based on matching the viscous solution to the MDR log-law in [46]. Note that the numbers appearing in Virk's law correspond to $\delta^+ = 5.85$, which is well within the error bar on the value of this Newtonian parameter. Note that we can easily predict where the asymptotic law turns into the viscous layer upon the approach to the wall.

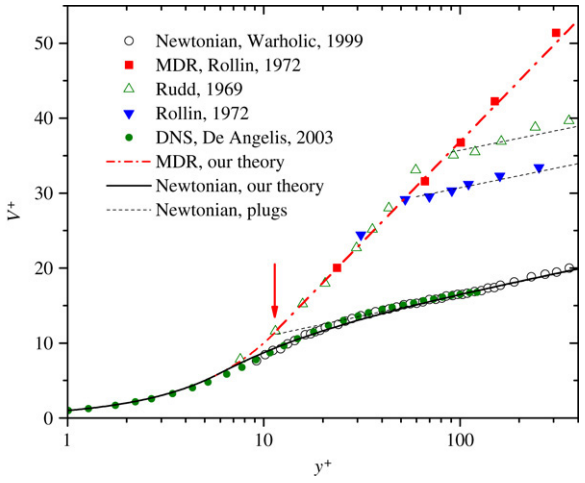

Fig. 4. Mean normalized velocity profiles as a function of the normalized distance from the wall during drag reduction. The data points from numerical simulations (green circles) [52] and the experimental points (open circles) [53] represent the Newtonian results. The black solid line is the universal Newtonian line which for large y^+ agrees with von-Kármán's logarithmic law of the wall (13). The red data points (squares) [54] represent the Maximum Drag Reduction (MDR) asymptote. The dashed red curve represents our theory for the profile which for large y^+ agrees with the universal law (25). The blue filled triangles [54] and green open triangles [55] represent the cross over, for intermediate concentrations of the polymer, from the MDR asymptote to the Newtonian plug. Our theory is not detailed enough to capture this cross over properly. (For interpretation of the references to colour in this figure legend, the reader is referred to the web version of this article.)

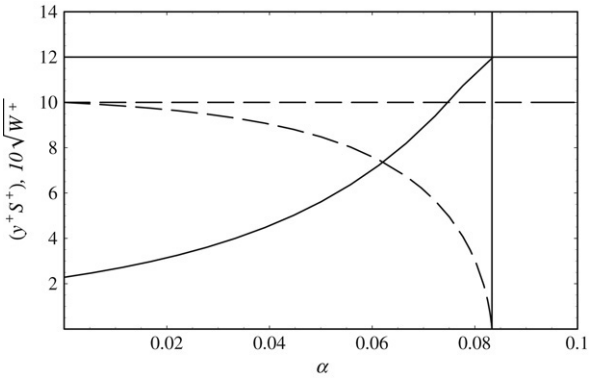

Fig. 5. The solution for $10\sqrt{W^+}$ (dashed line) and y^+S^+ (solid line) in the asymptotic region $y^+ \gg \delta^+$, as a function of α. The vertical solid line $\alpha = 1/2\delta^+ = 1/12$ which is the edge of turbulent solutions; Since $\sqrt{W^+}$ changes sign here, to the right of this line there are only laminar states. The horizontal solid line indicates the highest attainable value of the slope of the MDR logarithmic law $1/\kappa_V = 12$.

We can consider an infinitesimal W^+ and solve Eqs. (36) and (37) for S^+ and the viscosity profile. The result, as before, is $\nu^+(y) = \Delta(\alpha_m)y^+$. Since the effective viscosity cannot fall bellow the Newtonian limit $\nu^+ = 1$ we see that the MDR cannot go below $y^+ = \Delta(\alpha_m) = 2\delta^+$. We thus expect an extension of the viscous layer by a factor of 2, in very good agreement with the experimental data.

5.3. Non-universal aspects of drag reduction by polymers

When the concentration of polymers is not large enough, or when the Reynolds number is too low, the MDR is attained only up to some value of y^+ that depends in a non-universal manner on the Reynolds number and on the nature of the polymer [49]. These non-universal turn-backs to the so-called "Newtonian plug" can be understood theoretically, and we refer the reader to [44,50] for further details.

5.4. Drag reduction by micro-bubbles

Finally, we should mention that drag reduction by polymers is not the solution for many technologically pressing problems, the most prominent of which is the locomotion of ships. Here a more promising possibility is the drag reduction by bubbles, a subject that is much less developed than drag reduction by polymers. For some recent papers on this subject, see, for example [51] and the references therein; we stress that this subject is far from being exhausted by these papers, and expect more work to appear in the near future.

6. Thermal convection

Convection in Nature often occurs in conjunction with other physical effects such as rotation, magnetic field and particulate matter, so the knowledge of the subject is relevant to several closely related fields. The complexity of the underlying equations has precluded much analytical progress for circumstances of practical interest, and the demands of computing power are such that routine simulations have not yet been possible. Thus, the progress in the field has depended more on input from experiment, which has limitations of its own in terms of accessible parameter ranges. The progress in the subject, such as it is, has been possible only through strong interactions among theory, experiment and simulation. This is as it should be.

The paradigm for thermal convection is the Rayleigh–Bénard problem in which a thin fluid layer of infinite lateral extent is contained between two isothermal surfaces with the bottom surface maintained slightly hotter. When the expansion coefficient is positive (as is the case usually), an instability develops because the hot fluid from below rises to the top and the colder fluid from above sinks to the bottom. The applied driving force is measured in terms of a Rayleigh number, Ra,

$$Ra = g\alpha\Delta T H^3/\nu\kappa, \tag{46}$$

which emerges [56] as the appropriate non-dimensional measure of the imposed temperature difference across the fluid layer. Here, g is the acceleration due to gravity, H is the vertical distance between the top and bottom plates, α, ν and κ are, respectively, the isobaric thermal expansion coefficient, the kinematic viscosity and the thermal diffusivity of the fluid. Physically, the Rayleigh number measures the ratio of the rate of potential energy release due to buoyancy to the rate of its dissipation due to thermal and viscous diffusion.

The second important parameter is the Prandtl number

$$Pr = \nu/\kappa, \tag{47}$$

which is the ratio of time scales due to thermal diffusion ($\tau_\theta = H^2/\kappa$) and momentum diffusion ($\tau_\nu = H^2/\nu$), and

Table 1
Values of the combination of fluid properties $\alpha/\nu\kappa$ for air, water and helium [66]; SVP = saturated vapor pressure

Fluid	T (K)	P (Bar)	$\alpha/\nu\kappa$
Air	293	1	0.12
Water	293	1	14
Helium I	2.2	SVP	2.3×10^5
Helium II	1.8	SVP	–
Helium gas	5.25	2.36	6×10^9
Helium gas	4.4	2×10^{-4}	6×10^{-3}

determines the ratio of viscous and thermal boundary layers on the solid surfaces. With increasing Ra the dynamical state of the Rayleigh–Bénard system goes from a uniform and parallel roll pattern at the onset ($Ra \sim 10^3$) to turbulent state beyond Ra of 10^8, say.

For purposes of theoretical simplification, it is customary to assume that the thermal driving does not affect the pressure or the incompressibility condition, and that its only effect is to introduce buoyancy. This is the Boussinesq approximation. How closely the theoretical results correspond to observations depends on how closely the experiments obey the Boussinesq approximation. It is also not clear if small deviations from the ideal boundary conditions produce only small effects.

6.1. Experiments using cryogenic helium

Since many examples of convection occur at very high Rayleigh numbers [57], it is of interest to understand the heat transport characteristics in that limit. It is also necessary to be able to cover a large range of Ra in order to discover the applicable scaling laws. Cryogenic helium has been used successfully for the purpose. Though experiments in conventional fluids have been valuable [58,59], the Rayleigh number has been pushed to the limit only through the use of cryogenic helium. The same properties that make helium a suitable fluid for convection studies also makes it suitable for creating flows with very high Reynolds numbers [60].

Historically, a small "superfluid wind tunnel" was constructed [61] with the idea of exploiting the superfluid properties of helium II for obtaining very high Reynolds numbers. Potential flow was observed for low velocities, with no measurable lift on a pair of fly wings hanging in the tunnel, but the inevitable appearance of quantized vortices (see Section 7 on superfluid turbulence) altered that picture for higher flow speeds. Threlfall [62] recognized the advantages of using low temperature helium gas to study high-Ra convection. The later work by Libchaber and co-workers [63] brought broader awareness to the potential of helium. The work of Refs. [64,65] is a natural culmination of this cumulative effort. It is regrettable, though understandable, that the drive towards higher Rayleigh numbers has occurred in all these experiments at the sacrifice of the lateral extent of the apparatus (so the connection to the ideal Rayleigh–Bénard problem needs some justification).

The specific advantage of using helium for convection is the huge value of the combination $\alpha/\nu\kappa$ near the critical point. This can generate large Ra (see Table 1). For a fluid layer some 10 m tall and a reasonable temperature difference of 0.5 K, Rayleigh numbers of the order 10^{21} are possible. Table 1 also shows that $\alpha/\nu\kappa$ is quite small at pressures and temperatures sufficiently far away from the critical value. In fact, the range shown in the table covers a factor of 10^{12}, so any experiment of fixed size H can yield about 12 decades of the control parameter Ra by this means alone. However, if H is chosen to be large enough, this entire range of Ra can be shifted to a regime of developed turbulence where well-articulated scaling relations might be observed. This tunability is essentially impossible for air and water, especially because one cannot use more than modest temperature difference to increase Ra (due to the attendant non-Boussinesq effects, Section 6.3). For other advantages of using helium, see [66].

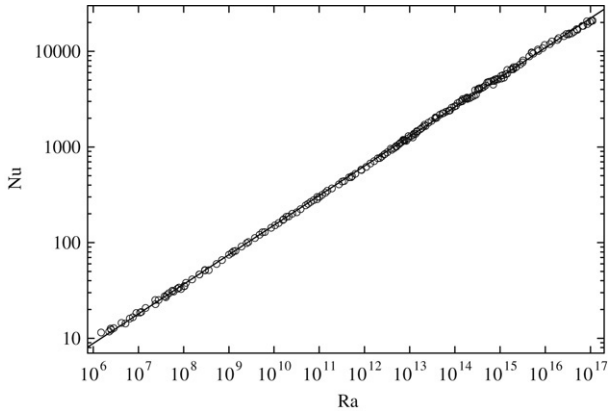

Fig. 6. Log–log plot of the Nusselt number versus Rayleigh number. The line through the data is a least-square fit over the entire Ra range, and represents a $\mathrm{d}\log Nu/\mathrm{d}\log Ra$ slope of 0.32.

6.2. The scaling of the heat transport

The heat transport in convection is usually expressed in terms of the Nusselt number Nu

$$Nu = \frac{q}{q_{cond}} = \frac{qH}{k_f \Delta T}, \tag{48}$$

where q is the total heat flux, q_{cond} is the heat flux in the absence of convection, given by Fourier's law, and k_f is the thermal conductivity of the fluid. Nu represents the ratio of the effective thermal conductivity of the fluid due to its turbulent motion to its molecular value. One goal of convection research is to determine the functional relation $Nu = f(Ra, Pr)$. This relation is at least as fundamental as the skin friction relation in isothermal flows.

Fig. 6, reproduced from Ref. [66], illustrates the enormous range of Ra and Nu that is possible in low temperature experiments of modest physical size (1 m height). The Nusselt numbers have been corrected here for sidewall conduction and also for finite thermal conductivity of the plates (and both corrections are small, see [66]). That Nusselt numbers attain values as high as 10^4 in these measurements is a testimony to the great practical importance of turbulence.

We have shown this figure partly because it represents the highest Ra achieved so far under laboratory conditions and also

the largest range of Ra in the turbulent scaling regime, both of which represent the fulfilment of the promise of cryogenic helium gas. The average power-law exponent over 11 decades is 0.32, close to $1/3$. We show this figure also because one might have hoped that such an unusual straight line spanning many decades in Ra might have a finality to it. Perhaps it does. However, experiments of Chavanne et al. [65], and by Niemela and Sreenivasan [67] for a different aspect ratio, have found a scaling exponent rising beyond $1/3$ towards the very highest Ra. The plausible conclusions of Niemela and Sreenivasan [67,68] were that those data corresponded to large non-Boussinesq conditions and to variable Prandtl number (which occur when one operates close to the critical point), but it is important to test these plausible conclusions directly. We shall momentarily discuss the current work in this direction. If we ignore the apparently non-Boussinesq regime, it has been argued in Refs. [67,68] that the scaling exponent from existing data is most likely consistent with a value close to $1/3$.

As already mentioned, computations have not yet approached experiments in terms of high Ra, but their advantage is that Pr can be held constant and the Boussinesq approximation can be enforced strictly. The available computational ability has recently been pushed by Amati et al. [69], who have reached Rayleigh numbers of 2×10^{14}. Even though this number is still about three orders of magnitude lower than the highest experimental value, it has become quite competitive with respect to many other experiments. This work suggests that the one-third exponent is quite likely, reinforcing the conclusion of Refs. [67,68]. Computational simulations have also explored the effects of finite conductivity, sidewall conduction and non-Boussinesq effects [70,71].

In spite of the limitations of Ra attainable in simulations, much of the details we know about boundary layers and fluctuations come from them. If one were to desire more of simulations (apart from nudging the ranges of Rayleigh and Prandtl numbers), it is that they should test the limits of resolution better. Direct knowledge of the velocity is most desirable in understanding the dynamics of plumes and boundary layers, and also the importance of the mean wind. Experiments in convection have limited themselves to measuring the mean wind and temperature at a few points, but not the spatial structures. The conventional techniques of velocity measurements and flow visualization are fraught with difficulties when considered for thermal convection in cryogenic helium, as has been discussed in [66].

We should now comment on the contributions of the theory to the heat transport problem. Two limiting cases for the scaling of Nu have been considered. The first scenario imagines that the global flux of heat is determined by processes occurring in the two thermal boundary layers at the top and bottom of the heated fluid layer. Then the intervening fluid, being fully turbulent and "randomized", acts as a thermal short circuit and therefore its precise nature is immaterial to the heat flux. We can then determine by dimensional arguments the relation to be $Nu \sim Ra^{1/3}$ [72]. This scaling assumes that the heat flux has no dependence on H. In the limit in which molecular properties are deemed irrelevant in determining heat transport – that is, when boundary layers cease to exist – an exponent of $1/2$ (modulo logarithmic corrections) has been worked out phenomenologically [73]. There has been an alternative theory [63] that obtains the $2/7$th scaling through intermediate asymptotics, but this aspect of the experimental result that motivated the work has not been sustained by more recent work.

The upperbound theory, though quite old (see Refs. [72,74]), has been taken to new levels through the efforts of Constantin and Doering (e.g., Ref. [75]), as well as by others more recently, and has contributed the following valuable hints on the heat transport law:

1. *Arbitrary Prandtl number:* $Nu < Ra^{1/2}$ uniformly in Prandtl number, Pr [75]. This result rules out dependencies such as $Pr^{1/2}$ [76,77] and $Pr^{-1/4}$ [73]. In particular, [73] was written when the boundary layer structure was understood much less than now, and there is a need to reconstruct its arguments afresh, in particular for the reassessment of the Rayleigh number at which the so-called "ultimate regime" with an exponent of $1/2$ is supposed to prevail for Prandtl numbers of the order unity.
2. *Large but finite Prandtl numbers:* The largeness of the Prandtl number is prescribed by the condition $Pr > cRa$, where c is a constant of the order unity. Under this condition, the upperbound is given by $Nu \leq Ra^{1/3}(\ln Ra)^{2/3}$ [78]. For higher Rayleigh numbers the upperbound is still given by (1) above.
3. *Infinite Prandtl number:* The latest result due to Doering et al. [79], is $Nu \leq CRa^{1/3}(\ln Ra)^{1/3}$. Robust calculations by Ireley et al. [80], which still seem to fall short of mathematical proof, is $Nu \leq aRa^{1/3}$, where a is a constant of the order unity.

Thus, as far as the upperbound theory is concerned, the $Ra^{1/2}$ result is permissible for Prandtl numbers of the order unity, though some semi-analytical results on Prandtl number dependencies are ruled out as noted in (1) above. Simulations suggest that the Nusselt number is independent of the Prandtl number above values of the order unity, so it is possible that the infinite Prandtl number limit already operates for unity values. The half-power seems likely when there are no boundary layers (such as in vertical pipes with no bottom and top boundaries), but there is also the continuing (though dwindling) hope of finding this behavior for "very large" Rayleigh numbers in a closed container. Exactly how large is "very large"? The notion that boundary layers will become irrelevant at very high Rayleigh numbers seems misconstrued to us.

Finally, we mention the effect of rough surfaces on the global heat transfer rate [81,82] and the presence of a weakly organized mean wind [83–86]. The studies just mentioned have added to our understanding of turbulent convection. The wind phenomenon has had a rather broad reach; e.g., quantitative observations of occasional reversals of the mean wind flow direction have been related to simple models of self-organized criticality [87]. Furthermore, the lifetimes of the metastable states of the bi-directional mean flow have intriguing analogies with reversals of the Earth's magnetic field polarity, a phenomena arising from turbulent convection within the outer

core [88]; there is also a quantitative statistical analogy with the lifetime of solar flare activity driven by turbulent convection in the Sun's outer layer [89]. This latter conclusion may indicate the existence of an underlying universality class, or a more direct physical similarity in the convective processes that lead to reshuffling of the magnetic footprints and to flare extinction.

6.3. Non-Boussinesq effects

One possible constraint for the Boussinesq condition to hold is that the fractional change in density across the layer,

$$\frac{\Delta\rho}{\rho} = \alpha\Delta T, \tag{49}$$

must be small. On the basis of a comparison to the Boussinesq problem at the onset of convection, it is generally assumed that values of $\alpha\Delta T < 0.2$, or less than 20% variation of density across the flow thickness, is acceptable. In the experiments this criterion is indeed satisfied up to very high values of Ra (up to 10^{15} for one set of data [67] and up to 10^{16} for another [64]), although there is no assurance that asymmetries of this magnitude are irrelevant at such high Ra. In fact, a more stringent requirement by a factor of 4 was adopted in Ref. [67].

Owing to the importance of non-Boussinesq effects, as discussed in Ref. [67], recent attention has been focused on them. An early exploration was by Wu and Libchaber [90], who reported top-bottom asymmetry in boundary layers as a main characteristic of non-Boussinesq effects, and observed, with increasing Ra, a reduction in the ratio of temperature drop across top boundary layer to that across the bottom boundary layer. Velocity profiles measured in a follow-up paper [91], at lower Ra, using glycerol, also showed an asymmetry. Ahlers and collaborators [92] showed that non-Boussinesq effects depend on the fluid, as one could readily expect. For water, Nu showed a modest decrease with increase in ΔT. For ethane, they found larger Nu than in the Boussinesq case, nearly 10% higher when $\alpha\Delta T = 0.2$.

As there are many possible non-Boussinesq effects and their relative importance depends on the fluid and its operating conditions, it is difficult to study these effects systematically in experiments. A numerical computation by [93] in two dimensions, using glycerol as the working fluid, showed that effects on Nu were marginal, with some decrease in Nu with $\alpha\Delta T$ for $Ra > 10^7$. In [71], these effects have been explored in three-dimensional convection, also computationally. The finding is that – at least for conditions corresponding to cryogenic helium gas at moderate Rayleigh numbers – while viscosity plays an important role in diminishing the movement of plumes to the interior of convection, it is the coefficient of thermal expansion that affects heat transport most.

6.4. Whither helium experiments?

While thermal convection has been studied for quite some time, the recent surge of interest – even in theory and simulations – has been triggered by helium experiments. Indeed, these experiments were ahead of theory and simulations about two decades ago. Since then, theory has been making its presence felt slowly and simulations have been making considerable inroads. Experiments have surely extended the parameter ranges, but, just as surely, they have not kept up the pace of sophistication. A major step in the understanding of the problem will occur only if accompanied by major improvement in experimental sophistication. It is therefore useful to take stock of the situation briefly. It is perhaps useful even to raise the question as to whether the promise of helium is realizable in its entirety anytime soon.

It has been recognized abundantly that the problem is with instrumentation and with probes of the desired temporal and spatial resolution. It is not clear to us that smaller probes based on the principles of standard thermal anemometry are the solution to the problem, part of which is that the use of helium raises the Reynolds number of the probe itself to higher values than in conventional fluids, leading to unfavorable (and poorly understood) heat transfer characteristics.

In thermal convection flows, where some direct knowledge of the velocity would be most desirable even at scales much larger than the Kolmogorov length, the use of hot and cold wires is further complicated by the fact that they require a steady flow – and the mean wind is effective only near the boundaries and also becomes weaker with Ra. Complications arise because the probe is sensitive simultaneously to temperature and velocity fluctuations in the environment.

Even if single-point measurements were successful, the need to measure the entire velocity field in a turbulent flow remains to be addressed. While a number of hot wires at several points can be used to obtain some spatial information, there is a limit to how far this procedure can be escalated. Particle Image Velocimetry (PIV) has been applied recently to liquid helium grid turbulence at 4.2 K [94,95], in counterflow turbulence [96] and in helium II turbulence [97]. However, the information has been obtained only in the form of two-dimensional sections, and time evolution of the flow cannot be assessed because of constraints of data acquisition. The PIV images do little justice to the three-dimensionality of the flow and to the enormous range of scales present at high Rayleigh numbers.

Particle selection and injection remain a fundamental hurdle for PIV measurements at low temperatures. Liquid helium has a relatively low density, and this makes it harder to find suitably buoyant particles that are also not too large. The use of hydrogen particles that match the density of helium has been the most promising step in this direction [97], but refined control of the particle generation is needed to render the technique routinely usable.

The seeding of helium gas for thermal convection experiments is probably even more difficult owing to the large variation of the density, and its nominally small value, which at best is less than half that of the liquid phase. As noted above, the liquid flow can be seeded to some level of adequacy but the price to pay is that the large range of Rayleigh numbers is attainable only in the gaseous phase.

Flow visualization can focus experimental – and even theoretical – efforts, and yet this domain has not been well developed for cryogenic helium. We believe that there is a

huge pay-off here because most existing flow visualizations in water and other room-temperature fluids are at low to moderate Rayleigh numbers, and the intuition that one derives from low Ra cannot easily be extended to high Ra. There are no technological barriers to perfecting the present efforts – only one of integrating various components together. We may also remark that it is not easy to test new particles in the actual low temperature environment. In experimental phase, White et al. [94] had resorted to testing in a pressurized SF_6 environment, where the density could be matched to that of liquid helium.

Where density gradients exist in the flow, visualization can occur in the absence of tracer particles, using shadowgraphy (which depends on the density gradient) or schlieren technique (which depends on the second derivative of the density). It has been demonstrated [98] that shadowgraphy can be used in helium I to visualize even weak flows near the convective onset. A light beam reflected from the cell displays intensity variations resulting from the convergence or divergence due to gradients in refractive index. Note that the technique does not give local information, but can be used to visualize only global flows. In the case of large apparatus, installing an optically transparent and thermally conducting plates is a nontrivial task.

For the case of turbulence under isothermal conditions, it would be possible to use helium 3 as a marker for shadowgraphs.

Scattering of ultrasound is another method that can in principle be used for velocity measurements in helium. It can be used in the gas phase which makes it a plausible candidate for cryogenic convection experiments. However, there would be substantial problems in achieving sufficiently high signal-to-noise ratio resulting from a mismatch of acoustic impedance between the sound transducers and the helium. The work in this direction [99,100] has not yet been adopted for cryogenic helium.

In summary, one part of the promise of helium (namely large values and ranges of the control parameters) has been delivered; flows with huge values of Ra and Re have indeed been generated in laboratory-sized apparatus. However, the second part of the promise (of being able to develop versatile techniques for precise measurements of velocity and vorticity) has lagged behind substantially, despite some impressive efforts. This is the aspect that needs financial investment and intellectual focus.

Once the instrumentation issues are clearer, we need to seriously consider an experiment that can combine moderate aspect ratio (say, 4) with high Ra, constant Pr, and Boussinesq conditions. Such an experiment is probably not without considerable technical difficulties. A large scale low temperature apparatus could be constructed, say at a facility like CERN or BNL, where there is adequate refrigeration capacity. Having a horizontal dimension of, say, 5 m or more would probably require some type of segmentation of the plates with multiplexing of the heating and temperature control. Fundamentally, this is no more complicated than the mirror arrays used in astrophysical observation. The bottom plate, which has a constant heat flux condition imposed, can be arbitrarily thick since it can be supported from below. The temperature control of the plate would probably be more difficult. Estimates for the cooling power required for cells of the size just mentioned seem well within the capacity of the existing refrigeration plants [66].

7. Superfluid turbulence

We now review some phenomenological aspects of liquid helium below the lambda point, called helium II. Helium II has a normal component and a superfluid component whose relative fractions depend on the temperature. The superfluid is frictionless at low flow velocities but enters, beyond a critical velocity, a state in which thin vortex lines are formed spontaneously. These line vortices align themselves with the axis of rotation if the container as a whole rotates, but otherwise form self-sustained tangles. The vortex lines move about in the background of elementary excitations or "quasi-particles" (which, in fact, form the normal component). The vortices scatter the excitations when there is relative velocity between them, thus generating the so-called mutual friction [101]. It was recognized by Onsager [102] that quantum mechanics constrains the circulation around the vortices to be $n\kappa/m$, where κ is Planck's constant and m is the mass of the helium atom; the integer $n = 1$ normally. However, the irrotational flow away from the core of the vortices, whose diameter is estimated to be of the order of an angstrom, is thought to be classical [103]. The motion produced by a vortex tangle, which can be quite complex because of the tangle's complex geometry, is called superfluid turbulence [104,105].

7.1. The $-5/3$ law and analogies to classical turbulence

One of the recent findings [106] is that turbulence in helium II has the Kolmogorov form for the spectral density with a well-defined $-5/3$ power, independent of whether the fraction of the superfluid is negligible or dominant. This result may not seem surprising if one takes the view that any nonlinearly interacting dissipative system of many scales will behave similarly to the classical Kolmogorov turbulence in the inertial range [1]: What is needed is merely the existence of mechanisms of excitation at some large scale and dissipation at the small scale, with no further detail mattering in the inertial range. However, several problems come to the fore when one examines possible scenarios for these mechanisms.

First the dissipation mechanism: Feynman [103] proposed a scenario by which vortex reconnections generate smaller and smaller loops in a cascade-like fashion, carrying energy away from larger scales. Vinen [107] suggested that the short wavelength Kelvin waves, which are created presumably by impulses associated with the reconnection of vortices, act as mediators of dissipation. For temperatures of 1 K and above, the Kelvin waves are damped out by the background excitations thus providing the dissipation mechanism. For lower temperatures, for which the normal fluid is negligible, the energy is radiated away as sound at sufficiently small wavelengths. There is follow-up work on the Kelvin-wave

mechanism for dissipation and on the nature of energy spectrum at very high wavenumbers (e.g., [108–110]; see also [105,111]) but the details are not yet fully understood. In particular, for energy loss by radiation to be effective, one needs very high velocities and short wavelengths: Modest motion of vortices will not do. Higher velocities are possible very close to the vortex core because of the inverse power-law of the potential velocity field – and also because of reconnection events, which produce cusp-like local structures with sharply repelling velocities.

Regarding the forcing scale, in experiments with a pull-through grid in helium II [112], it is conceivable that the forcing is produced very similarly to that in classical turbulence, and is related to the mesh length and the time of evolution of the turbulence. In simulations, on the other hand, the forcing scale cannot be defined unambiguously. For instance, in the important foray into superfluid turbulence that was made by Schwarz [113], it appears at first sight that the forcing scale was the size of the computational box, as also in the case of the simulations of the Taylor–Green problem by Nore et al. [114] and Araki et al. [115]. However, it appears that reconnections play an important role in determining this scale (or range of scales).

As another perspective on the same issue, the occurrence of the $-5/3$ spectrum in superfluid turbulence may be regarded as surprising if one takes the stand that the key mechanism for energy transfer across scales in hydrodynamic turbulence, namely vortex stretching, is absent in superfluid turbulence: No intensification and break-up due to vortex stretching is possible. It is the vortex break-up due to reconnections, not vortex stretching, that appears to be the key to the spectral distribution here. If this is true, it is interesting to speculate about the central importance attached to vortex stretching in classical turbulence.

To be sure, one should look closely at the veracity of claims about the $-5/3$ power-law. Our view is that the available evidence is too fragile to sustain the claim on the existence of the $-5/3$ spectrum in experiment or simulations. In experiments, the only real piece of evidence comes from [106], but at least to us it is not exactly clear what is being measured at the low end of the temperature (below 1 K), despite a good assessment in [104]. At slightly higher temperatures than 1 K, for which the available evidence for the $-5/3$ law also comes from [106], the data concern different fractions of superfluid and normal helium making it hard to disentangle the two. The measurements of [112], though intrinsically exciting in addition to having instigated the recent interest in the problem, are only indirectly supportive of the $-5/3$ law. Here, one measures the decay of superfluid vorticity (with certain caveats which are partially resolved by [116]) and notes that the behavior is similar to that of the classical vorticity. From this one can compute the energy dissipation rate and infer the classical Kolmogorov spectrum.

In simulations of superfluid turbulence, the result is unconvincing because the computational box size is still small. Here, we make a strong case for pushing the computational size to those that are currently the norm for classical turbulence.

Our conclusion is *not* that the $-5/3$ power is ruled out, but that the evidence is soft at present; one needs to produce more direct and convincing evidence.

There is another interesting wrinkle. If one assumes that the wavelength of the Kelvin waves which dissipate or radiate the energy are very small compared to the Kolmogorov scale, it is plausible to infer the spectral amplitude of fluctuations of superfluid velocity in the sub-Kolmogorov range. Presumably, the only relevant parameter in that range is the strain rate at the Kolmogorov scale, quite like the situation of the passive scalar spectrum at high Schmidt numbers. It then follows from dimensional reasoning that one should expect a -1 power for the spectrum in that region (see also [110]). On the other hand, decay data of superfluid vorticity were analyzed in [117] to suggest that the energy spectrum is consistent with a -3 power-law. This behavior is poorly understood at present.

7.2. Visualization of quantized vortex lines

An exciting development of recent few years is the visualization of quantized vortices and their reconnection using small neutral particles [97,118]. These particles are made by the *in situ* freezing of mixtures of hydrogen and helium. While these visualization studies have confirmed some interesting aspects of quantized vortices such as rings and reconnections, the particles are still too large compared with the diameter of the vortices (by a factor of about 10^4). Thus, while it is easy to convince oneself that the particles get attracted to vortex cores and decorate them, it is obvious that the particles are not always passive. One can calculate conditions under which the inertia of the particles has marginal influence on vortex lines, but there is no controlled means to ensure that this happens always: One would have to devise smaller particles before one can be confident of the fine details.

7.3. Concluding remarks on superfluid turbulence

At least in the initial stages when the study of superfluid turbulence was brought closer to classical turbulence community, one of the hopes was that it might be possible to create enormous Reynolds numbers in modest-sized facilities using helium II. However, it has turned out that the situation is no better than what is possible with helium I. The bottleneck is that the superfluid vorticity introduces an effective kinematic viscosity which is of the same order as the kinematic viscosity of helium I [104,111,112]. There indeed is a lot to learn and understand about superfluid turbulence as a subject of intrinsic interest. It is also likely that such knowledge offers new insights on classical turbulence.

A new direction of superfluid turbulence concerns helium 3 at much colder temperatures [119].

8. Final remarks

If we are interested in discovering laws underlying systems with many strongly interacting degrees of freedom and are far from equilibrium, it is important to begin with a study a few

of them with the same rigor and control for which particle physics, say, is well known. We can probably make the case that hydrodynamic turbulence, which arises in flowing fluids, is an ideal paradigm. Our first point is that the dynamical equations for the motion of fluids are known to great accuracy, which means that understanding their analytic structure can greatly supplement experimental queries; in just the same way, computer simulations – even if they require much investment of time and money – can be far more useful here than for many other problems of the condensed phase, in which the interaction potential among microscopic parts is often simply an educated guess. The stochasticity of turbulence (and of all systems that are driven hard) means that one may discern only laws that concern statistical behavior. If we are fortunate, these laws are universal in some well-understood sense. This is the way we regard the "problem of turbulence".

While we have not yet reached a state when we can declare victory (perhaps that may never happen in a strict sense), the "problem of turbulence" is being slowly chipped away by understanding, albeit partially, its several aspects. This review has touched a few aspects of the problem in which considerable progress has been made recently. There is, of course, much to do, and one needs to understand the richness of the problem and possess the discipline and focus needed to make a dent in one of its nontrivial aspects.

Acknowledgements

This work was supported in part by the US-Israel Binational Science Foundation. Section 6 has had significant input from Dr. J.J. Niemela.

References

[1] A.S. Monin, A.M. Yaglom, Statistical Fluid Mechanics, vol. II, MIT Press, 1971. Indeed, smaller scales than η are usually present because of intermittency, but we shall not consider this aspect here.
[2] G.I. Taylor, Proc. Roy. Soc. A 151 (1935) 421.
[3] V.S. L'vov, I. Procaccia, Phys. Rev. Lett. 76 (1996) 2896.
[4] V.I. Belinicher, V.S. L'vov, A. Pomyalov, I. Procaccia, J. Stat. Phys. 93 (1998) 797.
[5] V.S. L'vov, I. Procaccia, Phys. Rev. E 62 (2000) 8037.
[6] A.N. Kolmogorov, Dokl. Akad. Nauk. USSR 32 (1941) 16.
[7] R.H. Kraichnan, Phys. Fluids 11 (1968) 946.
[8] K. Gawedzki, A. Kupiainen, Phys. Rev. Lett. 75 (1995) 3608.
[9] M. Chertkov, G. Falkovich, I. Kolokolov, V. Lebedev, Phys. Rev. E 52 (1995) 4924.
[10] A. Pumir, B.I. Shraiman, E.D. Siggia, Phys. Rev. E 55 (1997) R1263.
[11] G. Falkovich, K. Gawedzk, M. Vergassola, Rev. Modern Phys. 73 (2001) 913.
[12] O. Gat, I. Procaccia, R. Zeitak, Phys. Rev. Lett. 80 (1998) 5536.
[13] I. Arad, I. Procaccia, Anomalous scaling in passive scalar advection and lagrangian shape dynamics, in: T. Kambe, (Ed.), IUTAM Symposium, 2001 pp. 175–184.
[14] A. Celani, M. Vergassola, Phys. Rev. Lett. 86 (2001) 424.
[15] I. Arad, L. Biferale, A. Celani, I. Procaccia, M. Vergassola, Phys. Rev. Lett. 87 (2001) 164502.
[16] Y. Cohen, T. Gilbert, I. Procaccia, Phys. Rev. E. 65 (2002) 026314.
[17] Y. Cohen, A. Pomyalov, I. Procaccia, Phys. Rev. E. 68 (2003) 036303.
[18] L. Angheluta, R. Benzi, L. Biferale, I. Procaccia, Phys. Rev. Lett. 97 (2006) 160601.
[19] S. Kurien, K.R. Sreenivasan, Measures of anisotropy and the universal properties of turbulence, in: New Trends in Turbulence, NATO Advanced Study Institute, Les Houches, Springer and EDP-Sciences, 2001, pp. 53–111;
L. Biferale, I. Procaccia, Phys. Rep. 414 (2–3) (2005) 43–164.
[20] I. Arad, V.S. L'vov, I. Procaccia, Phys. Rev. E 59 (1999) 6753.
[21] I. Arad, B. Dhruva, S. Kurien, V.S. L'vov, I. Procaccia, K.R. Sreenivasan, Phys. Rev. Lett. 81 (1998) 5330.
[22] I. Arad, L. Biferale, I. Mazzitelli, I. Procaccia, Phys. Rev. Lett. 82 (1999) 5040.
[23] I. Arad, V.S. L'vov, E. Podivilov, I. Procaccia, Phys. Rev. E 62 (2000) 4904.
[24] G.I. Barenblatt, J. Fluid Mech. 249 (1993) 513;
G.I. Barenblatt, A.J. Chorin, Phys. Fluids 10 (1998) 1043.
[25] K.R. Sreenivasan, A. Bershadskii, J. Fluid Mech. 554 (2006) 477.
[26] R.G. Moser, J. Kim, N.N. Mansour, Phys. Fluids 11 (1999) 943. DNS data at: http://www.tam.uiuc.edu/Faculty/Moser/channel.
[27] S. Hoyas, J. Jimenez, Phys. Fluids 18 (2006) 011702. DNS data at: http://torroja.dmt.upm.es/ftp/channels/.
[28] B.J. McKeon, J. Li, W. Jiang, J.F. Morrison, A.J. Smits, J. Fluid Mech. 501 (2004) 135. The data at: http://gasdyn.princeton.edu/data/e248/mckeon_data.html.
[29] A.J. Smits, M.V. Zagarola, Phys. Fluids 10 (1998) 1045;
M.V. Zagarola, A.E. Perry, A.J. Smits, Phys. Fluids 9 (1997) 2094;
M.V. Zagarola, A.J. Smits, Phys. Rev. Lett. 78 (1997) 239.
[30] W.K. George, Phil. Trans. R. Soc. A 365 (2007) 789.
[31] R.L. Panton, Phil. Trans. R. Soc. A 365 (2007) 733.
[32] P. Monkewitz, K.A. Chauhan, H.M. Nagib, Phys. Fluids (in press).
[33] V.S. L'vov, I Procaccia, O. Rudenko, Phys. Rev. Lett. (submitted for publication).
[34] S.B. Pope, Turbulent Flows, Cambridge, 2000.
[35] A.M.O. Smith, T. Cebeci, Douglas Aircraft Division Report DAC 33735, 1967.
[36] B.A. Toms, Proc. Internat. Congr. Rheology Amsterdam, vol. 2, North Holland, 1949, pp. 0.135–0.141.
[37] P.S. Virk, AIChE J. 21 (1975) 625.
[38] P.S. Virk, D.C. Sherma, D.L. Wagger, AIChE J. 43 (1997) 3257.
[39] K.R. Sreenivasan, C.M. White, J. Fluid Mech. 409 (2000) 149.
[40] J.L. Lumley, Annu. Rev. Fluid Mech. 1 (1969) 367.
[41] P.-G. de Gennes, Introduction to Polymer Dynamics, Cambridge, 1990.
[42] R.B. Bird, C.F. Curtiss, R.C. Armstrong, O. Hassager, Dynamics of Polymeric Fluids, vol. 2, Wiley, NY, 1987.
[43] A.N. Beris, B.J. Edwards, Thermodynamics of Flowing Systems with Internal Microstructure, Oxford University Press, NY, 1994.
[44] R. Benzi, E. De Angelis, V.S. L'vov, I. Procaccia, V. Tiberkevich, J. Fluid Mech. 551 (2006) 185.
[45] V.S. L'vov, A. Pomyalov, I. Procaccia, V. Tiberkevich, Phys. Rev. E 71 (2005) 016305.
[46] V.S. L'vov, A. Pomyalov, I. Procaccia, V. Tiberkevich, Phys. Rev. Lett. 92 (2004) 244503.
[47] E. De Angelis, C. Casciola, V.S. L'vov, A. Pomyalov, I. Procaccia, V. Tiberkevich, Phys. Rev. E 70 (2004) 055301.
[48] R. Benzi, E. deAngelis, V.S. L'vov, I. Procaccia, Phys. Rev. Lett. 95 (2005) 194502.
[49] H.J. Choi, S.T. Lim, P.-Y. Lai, C.K. Chan, Phys. Rev. Lett. 89 (2002) 088302.
[50] R. Benzi, V.S. L'vov, I. Procaccia, V. Tiberkevich, Europhys. Lett. 68 (2004) 825.
[51] T.S. Lo, V.S. L'vov, I. Procaccia, Phys. Rev. E 73 (2006) 036308.
[52] E. De Angelis, C.M. Casciola, V.S. L'vov, R. Piva, I. Procaccia, Phys. Rev. E 67 (2003) 056312.
[53] M.D. Warholic, H. Massah, T.J. Hanratty, Exp. Fluids 27 (1999) 461.
[54] A. Rollin, F.A. Seyer, Canad. J. Chem. Eng. 50 (1972) 714–718.
[55] M.J. Rudd, Nature 224 (1969) 587.
[56] D.J. Tritton, Physical Fluid Dynamics, Oxford, 1998.
[57] K.R. Sreenivasan, R.J. Donnelly, Adv. Appl. Mech. 37 (2001) 239–276.
[58] R.J. Goldstein, H.D. Chiang, D.L. See, J. Fluid Mech. 213 (1990) 111.

[59] G. Ahlers, Phys. Rev. E. 63 (2001) art. no. 015303;
E. Brown, A. Nikolaenko, D. Funfschilling, G. Ahlers, Phys. Fluids 17 (2005) 075108.
[60] B.J. McKeon, C.J. Swanson, M.V. Zagarola, R.J. Donnelly, A.J. Smits, J. Fluid Mech. 511 (2004) 41.
[61] P.P. Craig, J.R. Pellam, Phys. Rev. 108 (1957) 1109.
[62] D.C. Threlfall, J. Fluid. Mech. 67 (1975) 17.
[63] B. Castaing, G. Gunaratne, F. Heslot, L. Kadanoff, A. Libchaber, S. Thomae, X.-Z. Wu, S. Zaleski, G. Zanetti, J. Fluid Mech. 204 (1989) 1.
[64] J.J. Niemela, L. Skrbek, K.R. Sreenivasan, R.J. Donnelly, Nature 404 (2000) 837.
[65] X. Chavanne, F. Chilla, B. Chabaud, B. Castaing, B. Hebral, Phys. Fluids 13 (2001) 1300.
[66] J.J. Niemela, K.R. Sreenivasan, J. Low Temp. Phys. 143 (2006) 163.
[67] J.J. Niemela, K.R. Sreenivasan, J. Fluid Mech. 481 (2003) 355.
[68] J.J. Niemela, K.R. Sreenivasan, J. Fluid Mech. 557 (2006) 411.
[69] G. Amati, K. Koal, F. Massaioli, K.R. Sreenivasan, R. Verzicco, Phys. Fluids 17 (2005) 121710.
[70] R. Verzicco, J. Fluid Mech. 473 (2002) 201;
R. Verzicco, Phys. Fluids 16 (2004) 1965.
[71] A. Sameen, R. Verzicco, K.R. Sreenivasan, Phys. Scr. (submitted for publication).
[72] W.V.R. Malkus, Proc. Roy. Soc. Lond. A 225 (1954) 196;
W.V.R. Malkus, Stud. Appl. Math. 107 (2001) 325.
[73] R.H. Kraichnan, Phys. Fluids 5 (1962) 1374.
[74] L.N. Howard, in: H. Gortler (Ed.), Proc. 11th Intern. Cong. Appl. Mech., Springer, Berlin, 1966, p. 1109; Annu. Rev. Fluid Mech. 4 (1972) 473.
[75] P. Constantin, C.R. Doering, J. Stat. Phys. 94 (1999) 159.
[76] E.M. Spiegel, Ann. Rev. Astron. Astrophys. 9 (1971) 323.
[77] S. Grossmann, D. Lohse, Phys. Rev. Lett. 86 (2001) 3316.
[78] X. Wang, Bound on vertical heat transport at large Prandtl numbers, 2007, preprint.
[79] C.R. Doering, F. Otto, M.G. Rezikoff, J. Fluid Mech. 560 (2006) 229–241.
[80] G.R. Ireley, R.R. Kerswell, S.C. Plasting, J. Fluid Mech. 560 (2006) 159–227.
[81] Y.B. Du, P. Tong, Phys. Rev. Lett. 81 (1998) 987.
[82] P. Roche, B. Castaing, B. Chabaud, B. Hebral, J. Sommeria, Euro. Phys. J. 24 (2001) 405.
[83] J.J. Niemela, L. Skrbek, K.R. Sreenivasan, R.J. Donnelly, J. Fluid Mech. 449 (2001) 169.
[84] K.R. Sreenivasan, A. Bershadskii, J.J. Niemela, Phys. Rev. E 65 (2002) 056306.
[85] X.L. Qui, P. Tong, Phys. Rev. E 64 (2002) 036304.
[86] E. Villermaux, Phys. Rev. Lett. 75 (1995) 4618.
[87] K.R. Sreenivasan, A. Bershadskii, J.J. Niemela, Physica A 340 (2004) 574.
[88] G.A. Glatzmaier, R.C. Coe, L. Hongre, P.H. Roberts, Nature 401 (1999) 885.
[89] A. Bershadskii, J.J. Niemela, K.R. Sreenivasan, Phys. Lett. A 331 (2004) 15.
[90] X.-Z. Wu, A. Libchaber, Phys. Rev. A 43 (1991) 2833–2839.
[91] J. Zhang, S. Childress, A. Libchaber, Phys. Fluids 10 (1998) 1534–1536.
[92] G. Ahlers, E. Brown, F.F. Araujo, D. Funschilling, S. Grossmann, D. Lohse, J. Fluid Mech. 569 (2006) 409–445;
G. Ahlers, F.F. Araujo, D. Funschilling, S. Grossmann, D. Lohse, Phy. Rev. Lett. 98 (2007) 054501.
[93] K. Sugiyama, E. Calzavarini, S. Grossmann, D. Lohse, Europhys. Lett. 80 (2007) 34002.
[94] C.M. White, A.N. Karpetis, K.R. Sreenivasan, J. Fluid Mech. 452 (2002) 189.
[95] R.J. Donnelly, A.N. Karpetis, J.J. Niemela, K.R. Sreenivasan, W.F. Vinen, C.M. White, J. Low Temp. Phys. 126 (2002) 327.
[96] T. Zhang, S.W. Van Sciver, J. Low Temp. Phys. 138 (2005) 865.
[97] G.P. Bewley, D.P. Lathrop, K.R. Sreenivasan, Nature 441 (2006) 588.
[98] A.L. Woodcraft, P.G.J. Lucas, R.G. Matley, W.Y.T. Wong, in: R.J. Donnelly, K.R. Sreenivasan (Eds.), Ultra-High Reynolds Number Flows, 1999, p. 436;
R.G. Matley, W.Y.T. Wong, M.S. Thurlow, P.G.J. Lucas, M.J. Lees, O.J. Griffiths, A.L. Woodcraft, Phys. Rev. E 63 (2001) 045301.
[99] S. Siefer, V. Steinberg, Phys. Fluids 16 (2004) 1587.
[100] C. Baudet, S. Ciliberto, J.-F. Pinton, Phys. Rev. Lett. 67 (1991) 193.
[101] H.E. Hall, W.F. Vinen, Proc. Roy. Soc. A 238 (1956) 204.
[102] L. Onsager, Nuovo Cimento Suppl. 6 (1949) 249. Discussion on the paper by C.J. Gorter.
[103] R.P. Feynman, Prog. Low Temp. Phys., 1, North-Holland, 1955, p. 17.
[104] W.F. Vinen, J.J. Niemela, J. Low Temp. Phys. 128 (2002) 167.
[105] W.F. Vinen, R.J. Donnelly, Phys. Today 43 (2007) 43.
[106] J. Maurer, Tabeling, Europhys. Lett. 43 (1998) 29.
[107] W.F. Winen, Phys. Rev. B 61 (2000) 1410.
[108] V.S. L'vov, S.V. Nazarenko, O. Rudenko, Phys. Rev. B 76 (2007) 024520.
[109] V.B. Eltsov, A.I. Golov, R. de Graaf, R. Hänninen, M. Krusis, V.S. L'vov, R.E. Solntsev. arXiv:0708.1095v1[cond-mat.soft], 8 August 2007.
[110] E. Kozik, B. Svistunov. arXiv:cond-mat/0703047v3[cond-mat.other], 24 October 2007.
[111] P.M. Walmsley, A.I. Golov, H.E. Hall, A.A. Levchenko, W.F. Vinen. arXiv:0710.1033v2[cond-mat.other], 31 October 2007.
[112] S.R. Stalp, L. Skrbek, R.J. Donnelly, Phys. Rev. Lett. 82 (1999) 4831;
L. Skrbek, J.J. Niemela, R.J. Donnelly, Phys. Rev. Lett. 85 (2000) 4831;
S.R. Stalp, J.J. Niemela, W.F. Winen, R.J. Donnelly, Phys. Fluids 14 (2002) 1377.
[113] K.W. Schwarz, Phys. Rev. B 31 (1985) 5782; Phys. Rev. B 38 (1988) 2398.
[114] C. Nore, M. Abid, M.E. Brachet, Phys. Rev. Lett. 78 (1997) 3896.
[115] T. Araki, M. Tsubota, S.K. Nemirovskii, Phys. Rev. Lett. 89 (2002) 145301.
[116] T.V. Chagovets, A.V. Gordeev, L. Skrbek, Phys. Rev. E 76 (2007) 027301.
[117] L. Skrbek, J.J. Niemela, K.R. Sreenivasan, Phys. Rev. E 64 067301.
[118] G.P. Bewley, M.S. Paoletti, K.R. Sreenivasan, D.P. Lathrop, 2007 (submitted for publication).
[119] L. Skrbek, JETP Lett. 80 (2004) 474.